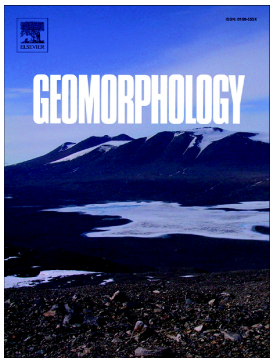

Structural and fluid-migration control on hill-hole pair formation: Evidence from high-resolution 3D seismic data from the SW Barents Sea

Benjamin Bellwald, Henrik Stokke, Monica Winsborrow, Sverre Planke, Joar Sættem, Nina Lebedeva-Ivanova, Amer Hafeez, Bartesz Kurjanski, Reidun Myklebust, Stéphane Polteau

PII: S0169-555X(22)00395-6

DOI: https://doi.org/10.1016/j.geomorph.2022.108502

Reference: GEOMOR 108502

To appear in: *Geomorphology*

Received date: 29 May 2022

Revised date: 19 October 2022

Accepted date: 19 October 2022

Please cite this article as: B. Bellwald, H. Stokke, M. Winsborrow, et al., Structural and fluid-migration control on hill-hole pair formation: Evidence from high-resolution 3D seismic data from the SW Barents Sea, *Geomorphology* (2022), https://doi.org/10.1016/j.geomorph.2022.108502

Structural and Fluid-Migration Control on Hill-Hole Pair Formation: Evidence from High-Resolution 3D Seismic Data from the SW Barents Sea

Benjamin Bellwald[1,2*], Henrik Stokke[1,3,4], Monica Winsborrow[4], Sverre Planke[1,5], Joar Sættem[6], Nina Lebedeva-Ivanova[1], Amer Hafeez[1**], Bartesz Kurjanski[7], Reidun Myklebust[8], Stéphane Polteau[9]

[1]Volcanic Basin Energy Research (VBER) AS, Høienhald, Blindernveien 5, 0361 Oslo, Norway (benjamin@vbpr.no), (henrik@vbpr.no), (planke@vbpr.no), (nina@vbpr.no)

[2]Department of Geosciences, University of Oslo, Oslo, Norway (benjamin.bellwald@geo.uio.no)

[3]Fjorgyn AS, Høienhald, Blindernveien 5, 0361 Oslo, Norway

[4]CAGE, Centre for Arctic Gas Hydrate, Environment and Climate, UiT The Arctic University of Norway, 9019 Tromsø, Norway (monica.winsborrow@uit.no)

[5]Centre for Earth Evolution and Dynamics (CEED), University of Oslo, Sem Sælands vei 1, 0371 Oslo, Norway (planke@vbpr.no)

[6]Independent (joarzm@online.no)

[7]University of Aberdeen, King's College, Aberdeen, AB24 3FX, UK (bkurjanski@abdn.ac.uk)

[8]TGS, Askekroken 11, 0277 Oslo, Norway

[9]Institute for Energy Technology (IFE), 2007 Kjeller, Norway (stephane.polteau@ife.no)

*Now at: Norwegian Geotechnical Institute (NGI)

**Now at: Vår Energy (amer.hafeez@varenergi.no)

Keywords

Hill-hole pair, fluid flow, shallow subsurface, fault, hydrocarbon reservoirs, Barents Sea, glaciotectonic, landform

Highlights

- Hill-hole pairs have been studied along a glacial unconformity in the SW Barents Sea
- There is an association between buried hill-hole pairs thermogenic hydrocarbons
- Localized basal freezing of the Barents Sea Ice Sheet occurs near fault terminations
- Hill-hole pairs above bedrock indicate a link to faults and hydrocarbon reservoirs

- Hill-hole pairs can be used as hydrocarbon seep indicators in petroleum exploration

Abstract

Hill-hole pairs are subglacial landforms consisting of thrust-block hills and associated source depressions. Formed by evacuation of material where ice-sheets have been locally frozen to the substrate, they give insights into paleo-ice-sheet dynamics. The aim of this study was to document the relationships between ancient hill-hole pairs identified on a buried glacial unconformity with the structure of the underlying sedimentary deposits, and then to determine if the basin geology and glacial fluid migration pathways, promoted local subglacial freeze-on during the hill-hole pair formation. The study is based on seismic geomorphological interpretation of four high-resolution 3D seismic cubes covering an area of 800 km^2 in the SW Barents Sea, and fluid seepage data from 37 gravity cores.

The seismic datasets allowed the identification of 35 hill-hole pairs along the buried unconformity. The hills are characterized by chaotic to homogeneous seismic facies forming up to 19 m high mounds, each covering areas of 2,000-644,000 m^2. The holes form depressions between 1-44 m deep and 2,000-704,000 m^2 in areal extent, which cut into preglacial Mesozoic bedrock and later infilled by glacial till. The holes are often found above fault terminations. High-amplitude reflections identified along the faults and in the strata below the holes are interpreted as shallow gas migrating upward towards the glacial unconformity. Geochemical data of the seabed sediment cores further indicates an association between hill-hole pair occurrence and present-day thermogenic hydrocarbon seepage.

The hill-hole pairs geometries were also used to identify five paleo-ice-flow directions along the glacial unconformity. These ice flows exhibit polythermal regimes, and four of them are parallel to ice-stream flow sets interpreted from glacial lineations. The integrated interpretation supports localized fault-related basal freezing of the Barents Sea Ice Sheet which resulted in the formation of hill-hole pairs when the ice sheet moved. In this context, the faults functioned as migration pathways for deep thermogenic fluids, possibly sourced from leaking Jurassic reservoirs.

This study highlights the importance of underlying geology for ice-sheet dynamics: While hill-hole pairs above glacial till appear to be commonly associated with dispersed gas hydrates, hill-hole pairs above bedrock additionally indicate a link to underlying fault systems and hydrocarbon reservoirs. Freeze-on of underlying bedrock to the basal ice along the strike of faults in sedimentary bedrock explains deeper hill-hole pairs with smaller extents along the glacial unconformity compared to areally larger but shallow hill-hole pairs detected above glacial till on modern seabeds. Such close association between paleo-thermogenic gas seepage and the location of hill-hole pairs strongly support that hill-hole pairs are excellent markers revealing exit points of fluid migration pathways in petroleum system models.

1. Introduction

Glaciotectonic processes are common both beneath and along the margins of ice sheets, and often leave characteristic landform assemblages in sedimentary rocks or unlithified sediments (Aber et al., 1989; Sættem et al., 1996; Aber and Ber, 2007; Evans et al., 2008; Rüther et al., 2013; Atkinson et al., 2014). Defined as the glacially-induced deformation (both ductile or brittle) of sediment or bedrock by glacial loading or movement, glaciotectonic landforms include megablocks, aligned rafts with well-preserved internal structure, moraine ridges influenced by ice push, glacial thrust blocks, and depressions, and hill-hole pairs (e.g., Solheim and Pfirman, 1985; Boulton, 1986; Moran et al., 1980; Sættem, 1990; Sættem, 1994; Andreassen et al., 2004; Rise et al., 2016; Evans et al., 2021). The diversity of glaciotectonic landforms reflects the wide range of processes involved over differing temporal and spatial scales. The nature of deformation is influenced by a range of variables, including substrate, basal thermal conditions, ice flow velocity, and meltwater availability.

Hill-hole pairs consist of thrust-block hills with associated source depressions, aligned sub-parallel to inferred ice-flow directions (Rise et al., 2016) (Fig. 1). The features are recognized on satellite images from terrestrial environments (Clayton and Moran, 1974; Moran et al., 1980; Bluemle and Clayton, 1984; Winsløw et al., 2020), and in bathymetric data from marine environments (Sættem, 1990;

Ottesen et al., 2005; Hogan et al., 2010; Rise et al., 2016; Bøe et al., 2016; King et al., 2016; Kurjanski et al., 2019) (Fig. 1). Hill-hole pairs form when subglacial sediments or bedrock are excavated and transported (usually for a short distance; 10s to 100s of meters) with the overlying ice, creating a hole from where the material has been sourced and a hill where it is subsequently deposited. This process implies the development of a decollement surface at some depth within the subglacial sediment or bedrock such that deformation occurs preferentially along this surface, rather than at the ice-bed interface.

In marine settings, many hill-hole pairs have been identified on shallow banks where relatively thin ice is likely to have been flowing slowly and sometimes frozen to the bed, with such basal freeze-on being favorable for glaciotectonic deformation (Ottesen et al., 2005; Ingólfsson et al., 2013; Dowdeswell et al., 2016). However, the first observations of offshore hill-hole pairs and other large-scale glaciotectonic structures were made in 200 to about 500 m below the present sea level in both bank and trough settings (Sættem, 1990; 1994), indicating that shallow water depth may not be the critical factor for glaciotectonics to occur. A growing number of such landforms (as well as glaciotectonic megablocks and rafts) are identified on ice-stream beds, which have been interpreted to reflect localized subglacial strong frictional bond (Winsborrow et al., 2016), consistent with the notion of ice-stream sticky spots (see Stokes et al. 2007 and reference therein).

In the Barents Sea, hill-hole pairs are commonly identified on ice-stream beds and interpreted to be related to subglacial gas-hydrate formation that provides favorable conditions for basal freeze-on and glaciotectonic deformation (Sættem, 1990; Sættem et al., 1994; Winsborrow et al., 2016). The high pore pressure and low temperature below ice sheets do indeed favor gas-hydrate growth (Lerche and Bagirov, 1998; Sloan, 2003), thus ice-covered areas overlying biogenic or thermogenic carbon sources have the potential to store large amounts of methane as hydrates. Furthermore, numerous pockmarks are present at the seabed in the area where hill-hole pairs are located, potentially indicating a link between abundant fluid flow from underlying pre-glacial bedrock (e.g., Bluemle and Clayton, 1984; Sættem, 1994; Tasianas et al., 2018). Deep-seated faults can facilitate focused fluid migration and fluid seepage (Eichhubl et al., 2000; Petersen et al., 2010; Geersen et al., 2016), and a link between a

deep-seated fault and a large hill-hole pair has been shown for the Alpha area in the SW Barents Sea (Bellwald et al., 2018a). Thus, if processes related to fluid flow do promote glaciotectonic deformation, we may expect a correlation between hill-hole pairs, deep-seated faults, and hydrocarbon reservoirs.

Hydrocarbon seep indicators are anomalous responses observed in geophysical, geological, and geochemical data and are interpreted to represent the presence of hydrocarbons. In seismic data, these indicators occur in different forms, such as amplitude strength and anomaly, and amplitude variation with offset that can be interpreted in terms of fluid contacts between gas, oil, and water. In exploration frontier areas, such as the Barents Sea, hydrocarbon seep indicators help boost confidence to drill a prospect and reduce exploration risks. Landform assemblages in the shallow subsurface are potentially valuable to assess active hydrocarbon systems at depth. These commonly include pockmarks, pipes, and vents that all indicate fluid migration from deeper reservoirs towards the seabed (Tasianas et al., 2018, Daszinnies et al., 2021).

Here we map the distribution of buried hill-hole pairs and evaluate if their distribution correlates with underlying faults and changes in basin stratigraphy. We further evaluate if such structures could be used for fluid migration, and thereby facilitate gas hydrate and associated hill-hole pair formation, and if hill-hole pairs can be used as a new hydrocarbon seep indicator. Previous studies on hill-hole pairs have mainly focused on their geometries using bathymetric data and conventional seismic datasets (Fig. 1; Ottesen et al., 2005; Klages et al., 2013; Rise et al., 2016; Kurjanski et al., 2019). Based on an integrated dataset of high-resolution 3D seismic data and sediment cores, we have now the opportunity to characterize hill-hole pairs along a bedrock-glacial till interface and investigate their link to underlying faults and fluid seepage features. We use these datasets to test the hypothesis if faults and gas-hydrates are the main mechanism by which the decollement process necessary to create hill-hole pairs may be facilitated. If a correlation between hill-hole pairs, deep-seated faults and facilitated fluid flow could be robustly established, this would provide valuable information for the analysis of active petroleum systems and deeper hydrocarbon accumulations and contribute to more robust site

characterizations and risk assessments for proposed offshore infrastructure along (paleo-)glaciated margins and sedimentary basins.

2. Study area

The SW Barents Sea is a shallow epicontinental shelf with water depths of 250-500 m (Fig. 2a), with its seafloor morphology greatly influenced by glacial erosion. Deep troughs, such as Bjørnøyrenna (Fig. 2a), formed during ice-streaming phases, as the Barents Sea Ice Sheet grew and decayed multiple times in the Pleistocene. The Bjørnøyrenna Ice Stream drained large amounts of ice from the central and northern Barents Sea to the western shelf edge (Fig. 2a) (Knies et al., 2009; Piasecka et al., 2016; Patton et al., 2017). Grounded ice left streamlined and erosional imprints (Sættem et al., 1992a, Andreassen et al., 2004), and deposited glacial till upon erosional surfaces and paleo-seabeds, as above the Upper Regional Unconformity (URU) which separates glacial sediments from the underlying preglacial rocks (Løseth et al., 1992; Bellwald et al., 2019). A grounded ice sheet is suggested to have formed in the present Barents Sea area from the Pliocene (c. 3.6 Ma), and continued to be periodically present throughout the Pleistocene, with multiple cycles of ice advance and retreat (Knies et al., 2009; Harishidayat et al., 2021). An intensification of northern hemisphere glaciations around 1-1.5 Ma resulted in repeated ice-sheet cover on the Barents Sea shelf (Knies et al., 2009).

The SW Barents Sea has been proven to be an active petroleum system with active fluid seepage but experienced a complex erosion and uplift history (Henriksen et al., 2011; Lasabuda et al., 2018; Tasianas et al., 2018; Ktenas et al., 2019). The study area is defined by four high-resolution 3D seismic cubes located between 73-74º N and 24-26º E (Fig. 2b). In the study area, the Hoop Fault Complex follows the general NE-SW to N-S trending faults of the Barents Sea (Collanega et al., 2017). The Hoop area is prospective for hydrocarbons (Fig. 2b; www.npd.no), and the major discoveries include Wisting, Sputnik and Apollo (all oil), and Gemini North, Atlantis, Norvarg and Mercury (all gas) (Fig. 2). Sands within the Jurassic Stø Formation are documented to have excellent reservoir properties (porosity and permeability) in the Hammerfest Basin (Dore, 1995). According to

some estimates, these sands could host up to 85% of the hydrocarbon reserves of the Norwegian Barents Sea (Larsen et al., 1993).

In the Hoop Fault Complex area of the SW Barents Sea, the URU is buried c. 20-70 m below the seabed and separates the Cretaceous bedrock of the Kolmule Formation from overlying Quaternary glacial till of the Nordland Formation (Bellwald et al., 2018b; 2019). The Cupola hills (Fig. 2a), consisting of mid-Cretaceous sedimentary bedrock and identified within the glacial package above URU, are the largest glaciotectonic landforms identified in the region (Sættem, 1994). Glaciotectonic deformation related to the Barents Sea Ice Sheet affected the uppermost 40 m of the Kolmule Formation (Bellwald et al., 2019). Modelling indicates that today, gas hydrates are only stable in the deepest parts of the troughs in the SW Barents Sea, down to c. 200 m below the seafloor (Vadakkepuliyambatta et al., 2017). However, in the presence of a thick ice sheet, gas hydrates are modelled to have been stable down to c. 450 m below seafloor across the entire Barents Sea, due to the high pressure-low temperature subglacial conditions (Andreassen et al., 2017). During glacial periods, interactions between the ice sheet and gas hydrate-fluid flow processes are hypothesized to have led to the formation of a variety of landforms, including glaciotectonic landforms and vast bedrock craters (Winsborrow et al., 2016; Andreassen et al., 2017; Waage et al., 2019; Bellwald et al., 2019).

Interpretation of 3D seismic data has allowed us to image a multitude of glacial landforms in the study area: Mega-scale glacial lineations, a shear margin moraine, shear band ridges, rhombohedral ridges and depressions, transverse ridges, iceberg ploughmarks, hill-hole pairs, pockmarks, and a braided river system (Piasecka et al., 2016; Bellwald et al., 2019; 2021; Bellwald and Planke, 2019).

3. Data and methods

3.1 Seismic data

Hill-hole pairs and their relationship with the underlying geology have been studied by using four P-Cable 3D seismic cubes located along the Hoop Fault Complex (Fig. 2b). The cubes measure 21x11 km (HFCE1), 25x3 km (HFCE2), 6x23 km (Alpha), and 24x15 km (Wisting). The P-Cable system for

HFCE1, HFCE2 and Alpha consisted of 16 streamers with lengths of 25 m and separated by 12.5 m. These data have been collected in 2014 using a single-source airgun with a volume of 300 in^3 and a shot point interval of 12.5 m. The migrated data have a dominant frequency of c. 120 Hz at URU depths (Lebedeva-Ivanova et al., 2018; Bellwald et al., 2019). Using a quarter of a wavelength as the resolution limit, landforms can be imaged with a vertical resolution of 3 m and a horizontal resolution of 6 m at URU depths (Fig. 3). The P-Cable system used for the Wisting cube consisted of 18 streamers with lengths of 100 m and separated by 12.5 m each. The data have been collected in 2016 using a double-source airgun with a volume of 300 in^3 and a shot point interval of 6.25 m. The data of the Wisting cube have a dominant frequency of c. 150 Hz at URU depths, and the stratigraphy can thus be imaged with a vertical resolution of c. 1 m and a horizontal resolution of 3 m (Fig. 4). Processing of the P-Cable data and resolution in the shallow subsurface are discussed in previous publications of the area (Lebedeva-Ivanova et al., 2018; Bellwald et al., 2019).

Otto (2017) stated that 3D seismic data at development stage facilitates the optimization of drilling processes, and that new standards in resolution are required. The structure maps and underlying geology of the P-Cable data have been compared with conventional 3D seismic data (Figs. 3, 4). The conventional data have been collected with a 3400 in^3 airgun and a streamer spread of 8 x 100 m x 6000 m, with resulting bin sizes of 12.5 x 25 m. The latest high-resolution 3D datasets used in this study image the subsurface in resolution superior to conventional 3D seismic data (Fig. 4), allowing mapping of faults to depths where conventional data lack sufficient resolution for the interpretation of geological structures.

3.2 Seismic interpretation

Every fourth inline of the URU horizon, which is characterized by a positive-amplitude reflection in the study area (Fig. 3a), has been picked for the first three datasets (HFCE1, HFCE2, Alpha). The URU horizon has been gridded, and the generated grid snapped to a horizon afterwards. The gridding was 4x4 m with a median filter of 3x3 cells for HFCE1, 4.75x4.75 m with a median filter of 15x15 cells for HFCE2, and 6.25x6.25 m with a median filter of 5x5 cells for Alpha. The maximum positive amplitude reflection of a vertical window of 5 ms (2.5 ms above and 2.5 ms below) around the

snapped horizon defines the used URU grid. All the seismic cubes used in this study have American polarity. In the illustrations in this paper reflections caused by an increase in acoustic impedance, positive-amplitude reflections, are shown as black in profiles while the opposite, reflections caused by a decrease in acoustic impedance, negative-amplitude reflections, are shown as white.

The interpretation of the Wisting cube was performed in the depth migrated P-Cable dataset TGS1600-4-PSDM. Every 16th inline and crossline have been picked manually by amplitude snapping (3 m window) for the entire cube, with every fourth inline and crossline interpreted in key areas where additional grid density was needed to ensure precision of interpretations. The horizon has been propagated based on the manually interpreted grid, followed by interpolation and surface snapping within a 1 m window to fill minor interpretation gaps that could not be propagated. The gridding was 3x3 m with a median filter of 5x5 cells for the Wisting cube.

Challenges in interpreting URU at such a high resolution are related to geometries (steeply dipping flanks), structures (interaction with polygonal faulting), sedimentological relationships (downlapping strata), and reflection seismic properties (acoustic impedance, bright spots, and presence of shallow gas). Improved imaging of the underlying faults has been achieved using frequency blending (30, 50, 80 Hz) along time slices.

3.3 Statistical analysis of hill-hole pair geometry

The principle of seismic geomorphology (Posamentier et al., 2007) was applied to define the geometries and dimensions of the hill-hole pairs, which then allowed statistical analysis of hill-hole pairs metrics and distribution. We only included geomorphic expressions which measured at least 100 m in one of the main axes, and smaller hill-hole pairs were not included in this work (Supplementary Table 1). Area, depth-to-height ratios and volume of every hill and hole were measured using ArcGIS after having imported the seismic horizons as 3D surfaces. Isolated holes with no associated hills are, based on the similarity in shape and location, also interpreted to be of glaciotectonic origin. In cases where both hills and holes are preserved, we determined the orientation of these pairs (Supplementary Table 1). The geometries of the hill-hole pairs are plotted on a logarithmic scale (due to their large

spread), and categorized into three areas (Gemini North, Wisting, Alpha) (Figs. 5-7). Producing the best fit of the data, we selected a power trendline for the data analysis, which is similar to the exponential curve, but has a more symmetrical arc. The hill-hole pairs identified in this study are compared with hill-hole pairs mapped on the present-day seafloor using multibeam swath bathymetry datasets available from the seafloor of the central Barents Sea (Kurjanski et al., 2019).

3.4 Sediment cores

A total of 37 gravity cores have been collected along a 41 km long sampling profile crossing the HFCEI seismic cube (Fig. 2b). The site spacing of the 58 to 226 cm long cores varies from 700 to 2000 m. The analyses focused on bio-chemical properties of the sampled material by using the commercial Microbial Prospecting for Oil and Gas (MPOG) method. MPOG is a surface exploration technology based on detection of significant populations of specific, hydrocarbon-degrading microorganisms in shallow soil samples, and in particular of methane-oxidizing bacteria. We used the MPOG results to evaluate the link between hill-hole pair occurrence and fluid migration from Mesozoic hydrocarbon reservoirs.

In addition, we used the Amplified Geochemical Imaging (AGI) method, which uses passive sampler technology to capture compounds in the C2-C20 range. All geochemical samples have been analyzed at the AGI laboratory in Elkton, Maryland, USA using an automated thermal desorption, gas chromatographic separation, and mass selective detection (ATD-GC/MS). These analyzes allow the detection and quantification of volatile and semi-volatile hydrocarbon compounds spanning from ethane (C_2) to octadecane (C_{18}), also including pristane (C_{19}) and phytane (C_{20}). The geochemical data have been evaluated for the presence and pattern of thermogenic hydrocarbons, indicative of active petroleum systems at depth in the area.

3.5 Fluid migration pathways

We integrate the geochemical results from the seabed sediment cores with the seismic data to interpret fluid migration pathways. Increased values of AGI and the sum of C_2-C_{14}, proxies gained from the seabed sampling, indicate fluid migration from deeper strata to the seafloor. Seismic data is the

primary tool for identifying fluid-charged layers and shallow gas over larger areas or in smaller accumulations, and common evaluation criteria are phase-reversed (negative polarity) reflections with anomalously high amplitudes (Heggland, 2004).

4. Results

The URU reflection in the Hoop area is defined as a continuous positive amplitude reflection in the seismic profiles (Fig. 3). A variety of glacial landforms with complex stratigraphic relationships are imaged in the URU structure maps of the high-resolution 3D seismic data. Pairs of ridges and depressions are striking features identified along URU in all the seismic cubes used in this study (Supplementary Figures 1-3). Based on their morphology, size and seismic facies, these types of landforms have previously been interpreted as hill-hole pairs (Bellwald et al., 2019).

The geometries of the 55 hill-hole pairs identified in this study are plotted in Figures 5-7, and the details of every pair are listed in Supplementary Table 1. The holes cover areas of 2,000 to 704,000 m^2, with a median of 16,000 m^2. The bottom of the 1 to 44 m deep holes (median depth of 9 m) is gently-dipping, and often follows subsurface reflections defining pre-existing geology (e.g., fault compartments, Fig. 3). The flanks of the holes are up to 60º steep, with average values of 20-40º. The volumes of the holes vary from 3,000 to 13,000,000 m^2, with a median of 95,000 m^2.

We identified an associated hill in close vicinity of 46 holes, and consequently nine out of 55 holes lack hills. The hills extend over 2,000 to 644,000 m^2 (median of 12,000 m^2) and are up to 12 m high but are often of insufficient height to interpret their internal structure and composition from the seismic data. However, deformation structures such as overthrusting are occasionally visible immediately adjacent to the hole (Fig. 3a). The hills have a low-gradient dipping angle (away from the holes) when tabular (Fig. 8b), and steeper angles when rim-shaped (Fig. 8c). The volumes of the hills are between 1,000 to 1,870,000 m^3 (median of 25,000 m^3), and the material shaping the positive relief of the hills has a similar volume to the topographic depression forming the associated hole. The relationship between the depth of the holes (y) and their extent (x) is $y = 0.406x^{0.31}$. The hills locally

co-exist with elongated grooves that are 1-5 km in length, 20-200 m in width, and 1-10 m in depth (Fig. 8).

4.1 Gemini North area (HFCE1 and HFCE2)

A total of 21 hill-hole pairs has been identified in datasets HFCE1 and HFCE2 in the Gemini North area. The holes cover areas from 3,000 to 124,000 m^2 and are 1 to 12 m deep. The hills extend from 3,000 to 205,000 m^2 with heights from 1 to 14 m (Fig. 5). The most prominent hole identified in the Gemini North area has a depth of 10 m and covers an area of 80,000 km^2 (Fig. 3). The pairs are NE-SW to SE-NW oriented (215 to 302º), and can be categorized into four clusters: a first cluster oriented from 215-218º (n: 3, ø: 217º , cluster A; ø: average), a second from 226-237º (n: 5, ø: 231º , B), a third from 247-257º (n: 3, ø: 252º , C), and a forth from 295-302º (n: 5, ø: 298º , D) (Fig. 7a). The morphologies of the hill-hole pairs in the HFCE1 cube vary from rectangular depressions with tabular ridges (Fig. 8b), to circular depressions with rims (Fig. 8c), and elongated depressions with small hills or lacking any hills (Fig. 9a).

A hill-hole pair consisting of two holes and a triangle-shaped hill is identified in the smaller cube (HFCE2, Fig. 10b). The 5 m deep holes, with a total extent of 38,000 m^2, correlate with an underlying polygonal fault. The E-W oriented hill pinches out towards the west and is a bit smaller in extent (35,000 m^2, or 92% of the holes), but shows continuous reflections indicating internal layering (Fig. 10b). Most of the holes in the 3D cubes of this study correlate with faults truncated at the URU level (Figs. 3, 9b, 10b). Time slices and frequency blends of the shallow subsurface below URU indicate that most of these structures are polygonal faults located within the Lower Cretaceous bedrock of the Kolmule Formation (Fig. 9c). While there is no association between glacial lineations and underlying faults, we observe a strong correlation between the hill-hole pairs and polygonal faults of HFCE1 (Fig. 9).

4.2 Wisting area

The structure map of the Wisting area is characterized by hill-hole pairs, mega-scale glacial lineations, and iceberg ploughmarks (Fig. 11). The quality of the high-resolution seismic cube allowed imaging of 33 hill-hole pairs. The holes have extensions from 2,000 to 118,000 m^2 with depths from 5 to 44 m. The hills cover areas from 2,000 to 70,000 m^2 and rise from 4 to 19 m (Fig. 5). While the holes have sharp flanks and strong seismic responses, the hills are poorly preserved and occasionally not present. The axes of the landforms with preserved hills and holes have dominating orientations of NE-SW to SE-NW, varying from 222-309º . These pairs can be categorized into four clusters: a first cluster oriented from 222-238º (n: 8, ø: 231º , cluster B), a second from 254-270º (n: 7, ø: 263º , C), a third from 279-283º (n: 2, ø: 281º , E), and a forth from 292-309 (n: 10, ø: 303º , D) (Fig. 7b). The orientation of the hill-hole-pair long axes is parallel to the orientation of the glacial lineations (Fig. 11b).

We document a strong link between the occurrence of the largest holes and faults (Figs. 12, 13). These faults can be deep-seated (several hundreds of meters deep) (Fig. 12) or shallow (meters to tens of meters deep) (Fig. 13). Polygonal faults around deeper faults are characterized by high-amplitude reflections around the fault planes (Fig. 13). The smaller, well-expressed hill-hole pairs show a correlation with underlying polygonal faults, with the extent of the holes overlapping the outline of the polygonal fault segments (Fig. 12).

4.3 Alpha area

The largest hill-hole pair of this study is identified in the Alpha 3D seismic cube (Fig. 14), which is the southernmost of the investigated datasets (Masiero, 2017). This hill-hole pair has a N-S-oriented depression, and an associated hill (9 m high and 644,000 m^2 in extent) to the east. The hole covers an area of 704,000 km^2 and consists of a 29 m deep depression (Fig. 14). The hole occurs above a deep-seated fault, and seismic anomalies are observed nearby (Fig. 14). Shallower faults originating from the deeper fault are identified in the north, where the seismic facies is rather chaotic. The stratigraphy to the south of the fault is characterized by continuous high-amplitude reflections. Similar to the

Wisting area, seismic anomalies are locally observed below URU around the hole (Figs. 13, 14), and in a deeper stratigraphic level next to the deeper fault below the hole. These anomalies could indicate migration and accumulation of fluids which escaped along the fault plane. If the faults functioned as a pathway, the bright spots below the URU could represent hydrocarbon accumulations related to fluid escape from the Late Mesozoic reservoirs.

5. Integration with shallow-core samples

The Hoop Fault Complex is underlain by hydrocarbon accumulations at different stratigraphic levels (Figs. 15, 16) (npd.no). In the case of HFCE1, flatspots within the Jurassic Stø Formation indicate the presence of hydrocarbons c. 150 m below URU. Strong phase-reversed seismic amplitudes are identified (i) 30 to 60 m below URU above all the reservoirs and to the east of Gemini East, (ii) directly below URU above the Sputnik and Gemini West reservoirs, and (iii) directly above URU above the Gemini North and Gemini East reservoirs as well as above URU to the east of Gemini East (Fig. 16). The strong phase-reversed seismic reflection above URU has a strong correlation with a shear margin moraine in the glacial sediment package and has been interpreted as a potentially fluid-charged, coarser-grained bed by Bellwald and Planke (2019).

Fluid migration from these reservoir levels to the seabed is detected by fluid analysis of seabed sediment cores (Fig. 15). We use both the AGI results and in particular the sum of ethane to tetradecane (sum C_2-C_{14}) from gravity-core sediment along a transect in the central part of HFCE1 (Fig. 15) as proxies for fluid seepage. The transect is located above tilted fault blocks, some of them displaying flat spots, as well as shallower amplitude anomalies (Fig. 16). The lithology of the cores is in general dominated by soft silty clay of dark gray, dark greenish gray, and gray color (5Y 4/1, 10 YR 4/2, 5GY 4/1, N4-N5). Elevated AGI values are measured over the Sputnik and Gemini East reservoirs, as well as in the area east of Gemini East (Figs. 15, 16). Increased C_2-C_{14} values are localized above the western part of the Sputnik field and to the east of the Gemini East reservoir (Fig. 16).

6. Discussion

The glacial unconformity (URU) has been formed by Quaternary glacial erosion and functioned as a former ice-stream bed in Bjørnøyrenna (Piasecka et al., 2016; Bellwald et al., 2019). The landform assemblage of this glacial surface, with frequently occurring hill-hole pairs, differs from classic ice-stream beds that tend to be dominated by streamlined, elongated grooves and lineations. In the following sections, we discuss hill-hole pair formation and geometries, their association with subsurface structures and fluid flow, as well as implication in constraining fluid migration pathways.

6.1 How do hill-hole pairs in the Barents Sea form?

We suggest that the 55 hill-hole pairs identified at URU within the SW Barents Sea have been formed by excavation of large blocks (median of 95,000 m^2 and 25,000 m^3, average of 447,000 m^2 and 109,000 m^3) of material from the paleo-seabed at locations where the Barents Sea Ice Sheet was frozen to the substrate, and where local conditions favored lift-off and decollement within the sub-ice sheet bedrock (Fig. 17a). The glaciotectonic erosion observed in our datasets removed up to 44 m of sedimentary bedrock, corresponding to a volume similar to the deposits building the thrusted blocks (Supplementary Table 1). The elongate and sub-circular depressions are thus interpreted to be the original locations of the thrusted material forming the hills deposited in the lee-side of the ice flow.

The hills of the landforms are often preserved, even when subsequently overridden. Deformation structures include overthrusting and even internal layering (Figs. 3, 10), the latter possibly representing thrust blocks broken into a series of imbricate slabs that appear as parallel ridges in the hill morphology (Fig. 10). Sediments forming the hills are likely pushed, stacked, or brecciated by compressive stresses (Fig. 17b). The hills represent mainly sedimentary material of the Cretaceous Kolmule Formation and show a similar reflection pattern as the cupola hills in the SW Barents Sea (Sættem, 1994). Such stresses are suggested to have been produced at the glacier bed and in the immediately underlying sediments by basal freezing and basal melting events, as suggested for landforms expressed on the glacier bed of the Prairie Region of North America (Moran et al., 1980).

Deformation structures are only imaged if their size is above seismic resolution and features smaller than 1-3 m are not resolved.

Excess pore water has been suggested to be drained from subglacial fine-grained sediments by basal freezing of ice sheets, leading to overconsolidation propagating downward from the base of the ice resulting in an inverted strength profile of otherwise homogenous fine-grained substratum and creating conditions favorable for tectonism (Sættem, 1990; Sættem et al., 1996; Christoffersen and Tulaczyk, 2003). Ice-lens-like features in frozen clay have been identified in borehole depths of 90 m in a suggested glaciotectonically affected area offshore mid-Norway (Sættem et al., 1996), and are associated with increasing gas content and decreasing shear strength in sediment. We suggest a decrease in pore pressure and increase in shear strength in the immediately underlying deformable sediments during freezing events (Fig. 17a). In contrast, increases in pore pressure and decreases in shear strength dominate during basal-ice melting (Fig. 17b). As proposed by Sættem (1994), we suggest glaciotectonic decollement to follow a layer of soft sediments beneath a stiffer, more consolidated interval. In our case, this decollement level is about 6-12 m below the seabed (Fig. 6a). This interpretation is further supported by soil property data from borehole cores which indicate layers of lower strength than above and below in otherwise similar clays (Sættem et al., 1992b) in the Svalis Dome area to the southwest of our study area (Fig. 2b). The shear strength versus depth in their data indicate a required stress of 10-20 kPa to create decollement at 6-12 m depth, which is reasonable in an ice-stream setting.

We note that pore-water drainage can reduce pore pressure dramatically by subglacial freeze-on under certain conditions (Fig. 17a) (Sættem et al., 1996). If such pore pressure drop reaches gas hydrate in the substratum, the hydrate may destabilize and release gas. Although this response will counteract the pore-pressured drop, it hints at the possible combination of a net freezing glacier bed (sticky), consolidation of subglacial sediments and underground decollement favored by the oscillation between the cracking forces of solid hydrate and free gas around the lower hydrate stability zone boundary across the Barents Sea (Andreassen et al., 2017). Seismic anomalies below the hill-hole

pairs could indicate that shallow gas is still present today (Figs. 13, 14). Gas migration to the seabed increased after the formation of the holes, as gas hydrate dissociated, and free gas escaped.

Glacial lineations expressed over some of the hills indicate glacier overriding (Figs. 3, 8, 11). The orientation of the hill-hole-pair axes, correlating with the direction of glacial lineations, allows reconstruction of past ice-flow directions, with the erosional hole formed upstream of the depositional hill (Fig. 7). We found a close association between parallel long axes of both glacial lineations and hill-hole pairs. A similar correlation between the directions of lineations and hill-hole pairs is also observed in Olga Strait, northern Barents Sea (Hogan et al., 2010). The orientation of four streamlined hill-hole pair clusters (clusters A, B, C, E) in our dataset are relicts from NNE-SSW and an E-W-oriented streaming events and correlate with lineation flow sets mapped over large extents at URU (Piasecka et al., 2016). The fifth cluster (cluster D), with average orientations of 298° in the Gemini North area and 303° in the Wisting area (Fig. 7), does not correlate with any previously mapped flow set, and might indicate a newly discovered ice-streaming event.

Ottesen et al. (2005) interpreted that the Norwegian margin submarine hill-hole pairs were linked to regions of slower-moving ice, possibly having formed during deglaciation. In North Dakota, thrust blocks have been interpreted to indicate frozen-bed conditions near the former ice margin (Clayton and Moran, 1974; Moran et al., 1980; Bluemle and Clayton, 1984). Ice-sheet configurations with frozen-bed conditions and slow-moving ice to ice stillstand are also prevailing during the formation of the hill-hole pairs identified in the SW Barents Sea, with a shear margin moraine located to the east of the area characterized by hill-hole pairs (Fig. 8) (Bellwald et al., 2018b; Bellwald and Planke, 2019).

The high-resolution 3D seismic data used in this study show that the distribution of hill-hole pairs at URU are fault-controlled, and we propose that these faults facilitated local glaciotectonic displacements. The high-amplitude reflections associated with the faults and seepage analysis in the sediment cores suggest that the faults were used as conduits for fluid migration where gas-hydrate formed at shallower levels. We further suggest that subglacial gas hydrate formation enhanced basal freeze-on and bulk strength of the substratum (Fig. 17a), as has been previously hypothesized for hill-hole pair formation in the Southern Barents Sea (Winsborrow et al., 2016). Indeed, gas hydrates

desiccate and stiffen host sediments permitting high basal traction between the ice and its bed, which is known to affect ice flow. Gas hydrates are reported in the modern subsurface of the Barents Sea (e.g., Vadakkapuliyambatta et al., 2017; Serov et al., 2017), and under glacial conditions of high pressure and low temperature, would likely have been far more extensive.

We suggest two types of formation processes for hill-hole pairs in the Barents Sea: A first type is focused fluid flow along faults building localized gas hydrates at bedrock-ice interfaces (Fig. 18a). The second type is fluid flow along faults getting diluted in the overburden, probably in combination with an inverted strength profiles in its upper part. This migration type results in dispersed gas hydrates in glacial till and evolving into a more random occurrence of hill-hole pairs at the seabed (Fig. 18b).

6.2 Glaciotectonic processes

Glaciotectonism results in ductile deformation for poorly lithified sediments, and brittle deformation for sedimentary bedrock (Andreassen et al., 2004; Aber and Ber, 2006). Glaciotectonized bedrock beneath URU is reported in two shallow stratigraphic boreholes in the study area (Sættem, 1991). The deformed reflections of moderate strength below URU have been interpreted as glaciotectonic deformed strata in previous studies (Bellwald et al., 2018; 2019). The eastwards-dipping reflections within the Cretaceous bedrock indicate a westward flowing Barents Sea Ice Sheet during the time of deformation. During multiple glacial advances, the loading and compaction of sediments and bedrock by ice resulted in deformed Cretaceous bedrock packages down to 30 m below URU (Fig. 9b). Deformed strata occur within the same fault segment, indicating normal faulting superimposed by later glaciotectonic deformation. Additionally, deformation is documented associated to the formation of mega-scale glacial lineations (Bellwald et al., 2019; Figs. 3a, 9b). Geometries similar to the glaciotectonically deformed strata of this study are conjugate normal faults developed in the Lønstrup Klint Formation with an offset of about 1 m (Pedersen, 2005).

6.3 Implications of hill-hole pair geometries

Well-preserved hill-hole pairs on the modern seabed were commonly formed during the last glaciation. These recent landforms display a variety of geometries but are often characterized by elongated tails on their lee-side (Sættem, 1990; King et al., 2016; Rise et al., 2016; Steinbitryggen-Sopphola in Fig. 1), which consist of glacial till (Sættem, 1990). For hill-hole pairs formed in glacial till, broad fault-guided patterns of fluid flow will determine in which areas gas hydrate formation is possible (Fig. 18). However, direct structural-control on the distribution of such hill-hole pairs is weaker than for those that directly overlay bedrock (i.e., URU hill-hole pairs), because gas hydrate in glacial till will tend to accumulate more randomly and more dispersed (Fig. 18). Furthermore, within laterally uniform clay-dominated till known from the SW Barents Sea (Sættem et al. 1992b), we suggest decollement could most easily occur beneath a consolidated layer attached to the base of the glacier ice. The expected shear strength below this layer increases with depth (e.g., Sættem et al., 1992a). Hence, thin layers are more easily displaced than thick ones. We may therefore expect larger hill-hole pairs but with a shallower extent.

In contrast, the URU hill-hole pairs are often not particularly well-defined. They are characterized by smaller extents and deeper holes and form a rim on the lee side of the hole or have a tabular shape (Figs. 3, 8, 11) when compared to the seabed hill-hole pairs (Fig. 6). Their less-pronounced relief might be a consequence of reduced preservation related to subsequent erosion and deformation. Here, we propose that their shapes reflect the distinct geology underlying the preserved URU hills compared to their seabed counterparts (Fig. 18). We argue that, in certain settings, the formation of gas hydrates subglacially may facilitate the formation of both seafloor and URU hill-hole pairs. We further suggest that the depth and nature of gas-hydrate distribution in the subglacial sediments/bedrock will influence the shape and position of the resultant hill-hole pair, with the depth of the hole broadly corresponding to the depth of the gas hydrate stability zone (Fig. 17a). Furthermore, the URU hill-hole pairs form at the interface between preglacial bedrock and glacial till. Here, in the underlying sedimentary bedrock, gas-hydrate accumulation is strongly linked to subsurface faults giving rise to a strong structural control on hill-hole pair formation and a smaller but deeper form (Weinberger and Brown, 2006; Cook et al., 2008).

Kurjanski et al. (2019) mapped 14 hill-hole pairs in the Central Barents Sea. The holes have average dimensions of 510 m x 860 m, extend over c. 0.6 km^2 (600,000 m^2) and are in average 7 m deep (Supplementary Table 1). The hills measure on average 300 m x 640 m in width/length and span over 0.3 km^2 (300,000 m^2) with average heights of 11 m (Fig. 6) (Kurjanski et al., 2019). Compared to the hill-hole pairs identified at the seabed of the Barents Sea, the URU hill-hole pairs have smaller lateral extensions, but deeper depressions (Fig. 6). The Alpha hill-hole pair (1.3 km^2) comes closest to compete in extent with the large hill-hole pair in Skagerrak (800 km^2, Ottesen et al., 2005), in Håkjerringdjupet (250 km^2, Sættem, 1994; Winsborrow et al., 2016), and on Fugløybanken (56 km^2, Sættem, 1990; Fig. 1).

The presence of gas hydrates is an important factor for the formation of both types of hill-hole pairs. While the gas hydrates within glacial till are likely to accumulate more randomly and more dispersed, these accumulations have a strong link to subsurface faults when located within sedimentary bedrock (Weinberger and Brown, 2006; Cook et al., 2008). As the distribution and formation of the hill-hole pairs at URU appear to be controlled by faults and gas hydrates, the depth of the hole gives a rough estimation about the depth of the gas hydrate stability zone (Fig. 17a). The depths of the holes are all located within the gas hydrate stability zone modelled for the SW Barents Sea (Vadakkepuliyambatta et al., 2017). Seismic anomalies in close vicinity to hill-hole pairs are interpreted as relicts of the paleo-gas hydrates (Figs. 13, 14), a model that has also been suggested for pockmark formation in the Norwegian Channel (Forsberg et al., 2007).

6.4 Hill-hole pairs and petroleum systems

A high-resolution 3D seismic cube with a densely-cored transect covering an area with several drilled hydrocarbon discoveries allow us to evaluate the significance of hill-hole pairs as evidence of fluid seepage similar to pockmarks and mud volcanoes (Fig. 16, Tab. 1). The hill-hole pairs in the Gemini North area occur west of a shear margin moraine, where the presence of mega-scale glacial lineations indicates streaming ice flow occurred across the URU surface (Fig. 15) (Piasecka et al., 2016; Bellwald et al., 2018b). The area is furthermore underlain by the Sputnik oil discovery (7324/6-1) c. 150 m below URU (Fig. 15). Similar discoveries are located below the shear margin moraine (7325/4-

1), where we see no evidence of ice streaming and no hill-hole pairs can be observed, we therefore infer that here the ice was flowing slower. The correlation between seabed fluid analysis, URU hill-hole pairs and hydrocarbon fields supports that the fluids for the gas hydrate formation and shallow gas accumulations most likely originate from Jurassic reservoirs. Fluids escaped from the sands of the Jurassic Stø Formation along Mesozoic fault planes. These fault planes thus functioned as fluid migration pathways with fluids migrating upwards and accumulating under the fault-plane-sealing URU. The fluids migrating from the Gemini West hydrocarbon field, located outside of the shear margin moraine, laterally deviate into the shear margin moraine on their way up to the seabed (Fig. 16). This lateral deviation in vertical fluid migration explains the lack of hill-hole pairs at URU level in an area directly above the Gemini West hydrocarbon field (Tab. 1; Fig. 15). The formation of the shear margin moraine hindered the ice to freeze into the underlying bedrock, and therefore hill-hole pairs could not form above the Gemini North and Gemini East hydrocarbon fields. However, fluid migration from these reservoirs is detectable in the seabed sediment cores (Figs. 15, 16).

Faults have been documented to be associated with gas hydrate and free gas accumulations (Weinberger and Brown, 2006; Cook et al., 2008), and the hill-hole pairs be used to locate the exit points of migration route, and hence provide valuable information to constrain petroleum systems. In our interpretations of hill-hole pair formation, fluids would migrate along faults, which connect deeper reservoirs to shallower gas-hydrate accumulations near the paleo-seabed. The overlying grounded Bjørnøyrenna Ice Stream locally and occasionally formed strong frictional bond to the gas hydrate-bearing sedimentary bedrock. The hill-hole pairs were formed when the ice ripped patches off its substratum (creating holes), and then depositing the excavated sediment/rocks from the holes downflow as hills when the decollement friction exceeded the bond to the overlying ice. In this context, the holes of the pairs represent local areas experiencing active fluid seepage, which was assisted by the faults. The accumulation of gas and gas hydrates could additionally weaken the affected underground, forming preferential decollement zones.

Our study highlights the correspondence between hill-hole pairs, faults, and hydrocarbon systems. A better knowledge on the distribution of hill-hole pairs and faults is a useful tool for predicting

hydrocarbon occurrence in datasets lacking any seep anomalies. Glaciotectonic landforms can thus show persistent fluid flow from the underlying basins. In the Barents Sea, fluid flow clearly influences glaciotectonic deformation and the formation of hill-hole pairs, and glaciotectonic deformation can here be used as a hydrocarbon indicator. Glaciotectonic deformation involving sticky spot and decollement should not only occur where hydrocarbons have migrated into affected strata in the Barents Sea, but also be far less common in areas not affected by the presence of hydrocarbons in the region.

6.5 Migration through the glacial package

Negative-amplitude anomalies above and below URU indicate that gas is temporarily stored at different levels below and above URU (Tab. 1). Fluids from the Gemini North and Gemini East blocks hit the shear margin moraine on their way up and could thus not form sticky spots for hill-hole pair formation. Fluid migration can be detected above Gemini East in sediment samples collected on the modern seafloor. This gas spike might be a combination of vertical migration along Gemini East and horizontally deviated fluid flow from Gemini North (Fig. 16, Tab. 1).

While the seabed in the Gemini North area is characterized by glacial lineations and some pockmarks (Bellwald et al., 2018b), the seabed in the Wisting area is dominated by iceberg ploughmarks and abundant unit pockmarks. Unit pockmarks are smaller in extent compared to normal pockmarks, 10s of meters wide, c. 1 m deep, and have a circular geometry (Hovland et al., 2002; Tasianas et al., 2018). Studies from the Snøhvit gas field conclude that unit pockmarks are formed by gas-hydrate dissociation after glaciation (Tasianas et al., 2018). The abundance of seabed pockmarks in both the Wisting and Gemini North area is thus another indicator that this region hosted gas hydrates in the shallow subsurface.

Our interpretations also show that fluid seepage occurs outside of a low-permeable shear margin moraine (Figs. 15, 16) (Bellwald and Planke, 2018). Therefore, this study also shows that glacial sediments can control fluid migration on small vertical scales. The identification of low-permeable

glacial deposits could be valuable for suitable site selection of carbon storage on glaciated margins, as these deposits can potentially prevent CO2 leakage.

7. Conclusions

The interpretation of high-resolution 3D seismic data allowed us to characterize buried hill-hole pairs formed by localized basal freeze-on of the Bjørnøyrenna Ice Stream and to establish links to underlying geological structures. Combining geophysical interpretations with gravity-core results documented a strong link between the presence of hill-hole pairs, fluid migration along different types of faults, and hydrocarbon reservoirs.

The 55 hill-hole pairs identified in this study, affecting subglacial bedrock strata, have extents from 8,000 to 1,350,000 m^2. They are thus an order of magnitude smaller than hill-hole pairs identified at the seabed and affecting Quaternary deposits. The depth of the holes at URU, however, is roughly double the depth of holes at the seabed.

The hill-hole pairs of the Gemini North area are all identified in an area with active paleo-ice streaming and correlate with the Sputnik hydrocarbon discovery c. 150 m below the paleo-seabed. The occurrence of these hill-hole pairs indicates the presence of localized frozen-bed conditions beneath parts of the former Barents Sea Ice Sheet. We suggest that increased vertical fluid flow from the Sputnik oil field fed the Cretaceous strata below the URU with gas, and the low-temperature, high-pressure subglacial conditions resulted in the formation of gas hydrates in these stratigraphic levels. Localized areas of basal freeze-on beneath a NE-SW to SE-NW flowing ice stream were formed where patches of subglacial gas hydrate existed, leading to the formation of the hill-hole pairs. Fluid seepage from the Sputnik discovery to the seabed is still ongoing today.

The absence of hill-hole pairs above the Gemini North and Gemini East hydrocarbon reservoirs can be explained by the formation of a shear margin moraine, indicating the absence of ice-streaming. Indications of gas migration can be found in glaciotectonically deformed beds below the URU, and a

soft bed above URU. However, gas from these reservoirs is still seeping to the seabed today but might undergo lateral migration along the glaciotectonic strata and the soft bed above URU.

Knowledge on ice-stream configurations, subglacial thermal regimes and glaciotectonic landforms are crucial for understanding seabed geochemical anomalies. Fluid seepage from Mesozoic reservoir rocks affects the formation of glacial landforms hundreds of meters above the reservoir. Links to subsurface structures and stratigraphy allow to draw conclusions about the genesis of different types of glacial terrains. Hill-hole pairs underlain by bedrock might have different formation process compared to the commonly detected hill-hole pairs along the seabed, which is usually underlain by glacial till.

High-resolution 3D seismic data are required to image small hill-hole pairs circa 10 times smaller in relief compared to the seabed. This quality of geophysical data is required to properly validate fluid migration and new hydrocarbon seep indicators at shallow subsurface levels.

Acknowledgements

We acknowledge TGS, OMV, Fjorgyn, and the Norwegian Petroleum Directorate for access to high-resolution 3D seismic cubes, and TGS and VBER for access to core data. We thank Edoardo Masiero for the interpretations on the Alpha 3D seismic cube as part of his Master Thesis, and Marija Rosenqvist for the support with conceptual sketches. Monica Winsborrow and Henrik Stokke acknowledge support from the Research Council of Norway (RCN) through its Centres of Excellence funding scheme, project no. 223259. Sverre Planke acknowledges the support from the Research Council of Norway (RCN) through its Centres of Excellence funding scheme, project 22325, as well as the ARCEx partners and RCN (grant number 228107). Stéphane Polteau acknowledges support from the RCN grant no. 331644 through the National Centre for Sustainable Subsurface Utilization of The Norwegian Continental Shelf.

References

Aber, J.S., Croot, D.G., Fenton, M.M., 1989. Hill-hole pair. Springer, Dordrecht, 13-28.

Aber, J.S., Ber, A., 2007. Glaciotectonism. Developments in Quaternary sciences, Elsevier, Amsterdam, 246 pp.

Andreassen, K., Nilssen, L.C., Rafaelsen, B., Kuilman, L., 2004. Three-dimensional seismic data from the Barents Sea reveal evidence of past ice streams and their dynamics. Geology 32(8), 729-732.

Andreassen, K., Ødegaard, C.M., Rafaelsen, B., 2007. Imprints of former ice streams, imaged and interpreted using industry three-dimansional seismic data from the south-western Barents Sea. In Davies, R.J., Posamentier, H.W., Wood, L.J., Cartwright, J.A. (Eds.). Seismic Geomorphology: Applications to Hydrocarbon Exploration and Production. Geological Society, London Special Publications 277, 151-169.

Andreassen, K., Winsborrow, M., 2009. Signature of ice streaming in Bjørnøyrenna, Polar North Atlantic, through the Pleistocene and implications for ice-stream dynamics. Annals of Glaciology, 50(52), 17-26.

Andreassen, K., Hubbard, A., Winsborrow, M., Patton, H., Vadakkepuliyambatta, S., Plaza-Faverola, A., ..., Bünz, S., 2017. Massive blow-out craters formed by hydrate-controlled methane expulsion from the Arctic seafloor. Science, 356(6341), 948-953.

Atkinson, N., Utting, D.J., Pawley, S.P., 2014. Glacial landforms of Alberta. Alberta Geological Survey, AER/AGS Map 604.

Bellwald, B., Planke, S., 2019. Shear margin moraine, mass transport deposits and soft beds revealed by high-resolution P-Cable three-dimensional seismic data in the Hoop area, Barents Sea. Geological Society, London, Special Publications, 477(1), 537-548.

Bellwald, B., Planke, S., Lebedeva-Ivanova, N., Piasecka, E.D., Andreassen, K., 2019. High-resolution Landform Assemblage along a Buried Glacio-erosive Surface in the SW Barents Sea Revealed by P-Cable 3D Seismic Data. Geomorphology 332, 33-50.

Bellwald, B., Planke, S., Lebedeva-Ivanova, N., Polteau, S., Lebedeva-Ivanova, N., Hafeez, A., Faleide, J.I., Myklebust, R., 2018a. Detailed Structure of Buried Glacial Landforms Revealed by High-resolution 3D Seismic Data in the SW Barents Sea. 80th EAGE Annual Conference and Exhibition 2018, Extended Abstracts 2018.

Bellwald, B., Planke, S., Piasecka, E.D., Matar, M.A., Andreassen, K., 2018b. Ice-stream dynamics of the SW Barents Sea revealed by high-resolution 3D seismic imaging of glacial deposits in the Hoop area. Marine Geology, 402, 165-183.

Bluemle, J.P., Clayton, L.E.E., 1984. Large-scale glacial thrusting and related processes in North Dakota. Boreas 13(3), 279-299.

Boulton, G.S., 1986. Push- moraines and glacier- contact fans in marine and terrestrial environments. Sedimentology, 33(5), 677-698.

Bøe, R., Ottesen, D., Rise, L., Dowdeswell, J.A., 2016. Streamlined ridges and depressions in the glacial sediments of the Arendal Terrace, Norwegian Skagerrak. In: Dowdeswell, J.A., Canals, M., Jakobsson, M., Todd, B.J., Dowdeswell, E.K., Hogan, K. (Eds.). Atlas of submarine glacial landforms: Modern, Quaternary and Ancient. Geological Society, London, Memoirs 46, 205-206.

Cartwright, J.A., 1994. Episodic basin-wide fluid expulsion from geopressured shale sequences in the north-sea basin. Geology 22, 447-450.

Cartwright, J., James, D., Bolton, A., 2003. The genesis of polygonal fault systems: a review. Subsurface Sediment Mobilization 216, 223-243.

Christoffersen, P., Tulaczyk, S., 2003. Thermodynamics of basal freeze-on: Predicting basal and subglacial signautres of stopped ice streams and interstream ridges. Annals of Glaciology 36, 233-243.

Clayton, L., Moran, S.R., 1974. A glacial process-form model. In: Coates, D.R. (Ed.), Glacial Geomorphology, State Univ. N.Y., Binghamton, Publ. Geomorphol., 89-119.

Collanega, L., Massironi, M., Breda, A., Kjølhamar, B.E., 2017. Onset of N-Atlantic rifting in the Hoop Fault Complex (SW Barents Sea): An orthorhombic dominated faulting? Tectonophysics 706, 59-70.

Cook, A.E., Goldberg, D., Kleinberg, R.L., 2008. Fracture controlled gas hydrate systems in the Gulf of Mexico. Marine and Petroleum Geology 25, 845-859.

Daszinnies, M., Plaza-Faverola, A., Sylta, Ø., Bünz, S., Mattingsdal, R., Tømmerås, A., Knies, J., 2021. The Plio-Pleistocene seepage history off western Svalbard inferred from 3D petroleum systems modelling. Marine and Petroleum Geology, 105023.

Dewhurst, D.N., Cartwright, J.A., Lonergan, L., 1999. The development of polygonal fault systems by synersis of colloidal sediment. Marine and Petroleum Geology 16, 793-810.

Doré, A.G., 1995. Barents Sea geology, petroleum resources and commercial potential. Arctic 4, 207-221

Dowdeswell, J.A., Hogan, K.A., Evans, J., Noormets, R., Cofaigh, C.O., Ottesen, D., 2010. Past ice-sheet flow east of Svalbard inferred from streamlined subglacial landforms. Geology 38, 163-166.

Dowdeswell, J.A., Canals, M., Jakobsson, M., Todd, B.J., Dowdeswell, E.K., Hogan, K.A., 2016. The variety and distribution of submarine glacial landforms and implications for ice-sheet reconstruction. Geological Society, London, Memoirs, 46(1), 519-552.

Eichhubl, P., Greene, H. G., Naehr, T., Maher, N., 2000. Structural control of fluid flow: offshore fluid seepage in the Santa Barbara Basin, California. Journal of Geochemical Exploration, 69, 545-549.

Evans, D.J.A., Clark, C.D., Rea, B.R., 2008. Landform and sediment imprints of fast glacier flow in the southwest Laurentide Ice Sheet. Journal of Quaternary Science 23, 249-272.

Evans, D.J., Phillips, E.R., Atkinson, N., 2021. Glacitectonic rafts and their role in the generation of Quaternary subglacial bedforms and deposits. Quaternary Research, 1-35.

Forsberg, C.F., Planke, S., Tjelta, T.I., Svano, G., Strout, J.M., Svensen, H., 2007 Formation of pockmarks in the Norwegian Channel. Offshore Site Investigation and Geotechnics, Confronting New Challenges and Sharing Knowledge. Society of Underwater Technology. 10pp.

Gales, J., Hillenbrand, C.D., Larter, R., Laberg, J.S., Melles, M., Benetti, S., Passchier, S., 2019. Processes influencing differences in Arctic and Antarctic Trough Mouth Fan sedimentology. Geological Society of London, Special Publications 475(1), 203-221.

Geersen, J., Scholz, F., Linke, P., Schmidt, M., Lange, D., Behrmann, J. H., ..., Hensen, C., 2016. Fault zone controlled seafloor methane seepage in the rupture area of the 2010 Maule earthquake, Central Chile. Geochemistry, Geophysics, Geosystems, 17(11), 4802-4813.

Heggland, R., 2004. Definition of geohazards in exploration 3-D seismic data using attributes and neural-network analysis. AAPG Bulletin, 88(6), 857-868.

Henriksen, E., Bjørnseth, H. M., Hals, T. K., Heide, T., Kiryukhina, T., Kløvjan, O. S., Stoupakova, A., 2011. Uplift and erosion of the greater Barents Sea: impact on prospectivity and petroleum systems. Geological Society, London, Memoirs, 35(1), 271-281.

Hogan, K.A., Dowdeswell, J.A., Noormets, R., Evans, J., O Cofaigh, C., 2010. Evidence for full-glacial flow and retreat of the Late Weichselian Ice Sheet from the water around Kong Karls Land, eastern Svalbard. Quaternary Science Reviews, 29, 3563-3582.

Hovland, M., Gardner, J.V., Judd, A.G., 2002. The significance of pockmarks to understanding fluid flow processes and geohazards. Geofluids 2, 127-136.King, E.L., Rise, L., Bellec, V.K., 2016. Crescentic submarine hills and holes produced by iceberg calving and rotation. In: Dowdeswell, J.A., Canals, M., Jakobsson, M., Todd, B.J., Dowdeswell, E.K., Hogan, K. (Eds.), Atlas of submarine glacial landforms: Modern, Quaternary and Ancient. Geological Society, London, Memoirs 46, 267-268.

Klages, J.P., Kuhn, G., Hillenbrand, C.D., Graham, A.G. C., Smith, J.A., Larter, R.D., & Gohl, K., 2013. First geomorphological record and glacial history of an inter-ice stream ridge on the West Antarctic continental shelf. Quaternary Science Reviews, 61, 47-61.

Knies, J., Matthiessen, J., Vogt, C., Laberg, J.S., Hjelstuen, B.O., Smelror, M., ..., Vorren, T.O., 2009. The Plio-Pleistocene glaciation of the Barents Sea–Svalbard region: a new model based on revised chronostratigraphy. Quaternary Science Reviews, 28(9-10), 812-829.

Ktenas, D., Henriksen, E., Meisingset, I., Nielsen, J.K., Andreassen, K., 2017. Quantification of the magnitude of net erosion in the southwest Barents Sea using sonic velocities and compaction trends in shales and sandstones. Marine and Petroleum Geology, 88, 826-844.

Kurjanski, B., Rea, B.R., Spagnolo, M., Winsborrow, M., Cornwell, D.G., Andreassen, K., Howell, J., 2019. Morphological evidence for marine ice stream shutdown, central Barents Sea. Marine Geology, 414, 64-76.

Larsen, R.M., Fjæran, T., Skarpnes, O., 1993. Hydrocarbon potential of the Norwegian Barents Sea based on recent well results. In: Vorren, T.O. et al. (eds.). Arctic Geology and Petroleum Potential. Norwegian Petroleum Society (NPF) Special Publication 2, Elsevier, Amsterdam, 321-331.

Lasabuda, A., Laberg, J.S., Knutsen, S.M., Høgseth, G., (2018). Early to middle Cenozoic paleoenvironment and erosion estimates of the southwestern Barents Sea: Insights from a regional mass-balance approach. Marine and petroleum Geology, 96, 501-521.

Lebedeva-Ivanova, N., Polteau, S., Bellwald, B., Planke, S., Berndt, C., Stokke, H.H., 2018. Toward one-meter resolution in 3D seismic. The Leading Edge 37, 818-828.

Lerche, I., Bagirov, E., 1998. Guide to gas hydrate stability in various geological settings. Marine and Petroleum Geology 15(5), 427-437.

Løseth, H., Lippard, S.J., Sættem, J., Fanavoll, S., Fjerdingstad, V., Leith, L.T., Ritter, U., Smelror, M., Sylta, Ø. 1993. Cenozoic uplift and erosion of the Barents Sea - Evidence from the Svalis

Dome area. In Norwegian Petroleum Society Special Publications (Vol. 2, pp. 643-664). Elsevier.

Masiero, E., 2017. The role of faults as potential traps for hydrocarbons in the late Mesozoic succession of the Alpha structure area (SW Barents Sea) highlighted by high resolution 3D seismics. Master Thesis, Universita degli studi di Padova, Italia. 73pp.

Moran, S.R., Clayton, I., Hooke, R.LeB., Fenton, M.M., Andriashek, L.D., 1980. Glacierbed landforms of the prairie region of North America. Journal of Glaciology, 25, 457-476.

Nygård, A., Sejrup, H.P., Haflidason, H., Bryn, P., 2005. The glacial North Sea Fan, southern Norwegian Margin: architecture and evolution from the upper continental slope to the deep-sea basin. Marine and Petroleum Geology 22, 71-84.

Ottesen, D., Dowdeswell, J.A., Rise, L., 2005. Submarine landforms and the reconstruction of fast-flowing ice streams within a large Quaternary ice sheet: the 2500-km-long Norwegian-Svalbard margin (57-80 N). GSA Bulletin 117(7-8), 1033-1050.

Otto, C., 2017. The importance of detailed geological characterization for future expanded use of gas storage in the sustainable energy context. Petroleum Geoscience 23(3), 327-338.

Patton, H., Hubbard, A., Andreassen, K., Winsborrow, M., Stroeven, A.P., 2016. The build-up, and dynamical sensitivity of the Eurasian ice-sheet complex to Late Weichselian climatic and oceanic forcing. Quaternary Science Reviews 153, 97-121.

Patton, H., Hubbard, A., Andreassen, K., Auriac, A., Whitehouse, P.L., Stroeven, A.P., Shackleton, C., Winsborrow, M., Heyman, J., Hall, A.M., 2017. Deglaciation of the Eurasian ice sheet complex. Quaternary Science Reviews 169, 148 - 172.

Piasecka, E.D., Winsborrow, M.C.M., Andreassen, K., Stokes, C.R., 2016. Reconstructing the retreat dynamics of the Bjørnøyrenna Ice Stream based on new 3D seismic data from the central Barents Sea. Quaternary Science Reviews 151, 212-227.

Pedersen, S.A.S., 2005. Structural analysis of the Rubjerg Knude Glaciotectonic Complex, Vendsyssel, northern Denmark. Geological Survey of Denmark and Greenland Bulletin 8, 192

pp. Petersen, C.J., Bünz, S., Hustoft, S., Mienert, J., Klaeschen, D., 2010. High-resolution P-Cable 3D seismic imaging of gas chimney structures in gas hydrated sediments of an Arctic sediment drift. Marine and Petroleum Geology, 27(9), 1981-1994.

Posamentier, H.W., Davies, R.J., Cartwright, J.A., Wood, L., 2007. Seismic geomorphology – an overview. Geological Society, London, Special Publications 277, 1-14.

Rise, L., Bellec, V.K., Ottesen, D., Bøe, R., Thorsnes, T., 2016. Hill-hole pairs on the Norwegian continental shelf. In: Dowdeswell, J.A., Canals, M., Jakobsson, M., Todd, B.J., Dowdeswell, E.K., Hogan, K. (Eds.), Atlas of submarine glacial landforms: Modern, Quaternary and Ancient. Geological Society, London, Memoirs 46, 203-204.

Rüther, D. C., Andreassen, K., Spagnolo, M., 2013. Aligned glaciotectonic rafts on the central Barents Sea seafloor revealing extensive glaciotectonic erosion during the last deglaciation, Geophysical Research Letters 40, 6351– 6355.

Serov, P., Vadakkepuliyambatta, S., Mienert, J. Patton, H., Portnov, A., Silyakova, A., Panieri, G., Carroll, M.L., Carroll, J., Andreassen, K., Hubbard, A., 2017. Postglacial response of Artic Ocean gas hydrates to climatic amelioration. Proceedings of the National Academy of Sciences, 114(24), 6215-6220.

Sloan, E.D., 2003. Fundamental principles and applications of natural gas hydrates. Nature, 426(6964), 353-359.

Solheim, A., Pfirman, S.L., 1985) Sea-floor morphology outside a grounded, surging glacier; Bråsvellbreen, Svalbard. Marine Geology, 65(1-2), 127-143.

Stokes, C.R., Clark, C.D., Lian, O.B., Tulaczyk, S., 2007. Ice stream sticky spots: a review of their identification and influence beneath contemporary and palaeo-ice streams. Earth-Science Reviews 81(3-4), 217-249.

Sættem, J., 1990. Glaciotectonic forms and structures on the Norwegian continental shelf: Observations, processes and impliactions. Norsk Geologisk Tidsskrift, 70, 81-94.

Sættem, J., 1991. Glaciotectonism – an important process in Late Cenozoic erosion in the southwestern Barents Sea. In J. Sættem (ed), Glaciotectonics and glacial geology of the southwestern Barents Sea. Dr. Ing. Thesis, Norwegian Institute of Technology, University of Trondheim, 75-115.

Sættem, J., 1994. Glaciotectonic structures along the southern Barents shelf margin. In: Formation and Deformation of Glacial Deposits (eds Warren, C. R. & Croot, D. C.) 95113 (Balkema, 1994), 95-113.

Sættem, J., Poole, D.A.R., Ellingsen, L., Sejrup, H.P., 1992a. Glacial geology of outer Bjørnøyrenna, southwestern Barents Sea. Marine Geology 103, 15-51.

Sættem, J., Rise, L., Westgaard, D.A., 1992b. Composition and properties of glacigenic sediments in the Southwestern Barents Sea. Marine Geotechnology 10, 229-255.

Sættem, J., Rise, L., Rokoengen, K., By, T., 1996. Soil investigations, offshore mid Norway: A case study of glacial influence on geotechnical properties. Global and Planetary Change 12(1-4), 271-285.

Tasianas, A., Bünz, S., Bellwald, B., Hammer, Ø., Planke, S., Lebedeva-Ivanova, N., Krassakis, P., 2018. High-resolution 3D seismic study of pockmarks and shallow fluid flow systems at the Snøhvit hydrocarbon field in the SW Barents Sea. Marine Geology, 403, 247-261.

Vadakkepuliyambatta, S., Chand, S., Bünz, S., 2017. The history and future trends of ocean warming- induced gas hydrate dissociation in the SW Barents Sea. Geophysical Research Letters 44(2), 835-844.

Waage, M., Portnov, A., Serov, P., Bünz, S., Waghorn, K.A., Vadakkepuliyambatta, S., ... Andreassen, K., 2019. Geological controls on fluid flow and gas hydrate pingo development on the Barents Sea margin. Geochemistry, Geophysics, Geosystems 20(2), 630-650.

Weinberger, J.L., Brown, K.M., 2006. Fracture networks and hydrate distribution at Hydrate Ridge, Oregon. Earth and Planetary Science Letters 245, 123-136.

Winsborrow, M.C.M., Andreassen, K., Hubbard, A., Plaza-Faverola, A., Gudlaugsson, E., Patton, H., 2016. Regulation of ice stream flow through subglacial formation of gas hydrates. Nature Geoscience 9, 370-374.

Winsløw, L.B., Pedersen, S.A.S., Boldreel, L.O., Nørmark, E., 2020. Wrench-fault structures superimposed by glaciotectonic complexes, interpreted from high-resolution reflection-seismic sections and boreholes along the western bank of Esrum Sø, north-east Sjælland, Denmark. Bulletin of the Geological Society of Denmark, 68, 171-193.

Wrona, T., Magee, C., Jackson, C.A., Huuse, M., Taylor, K.G., 2017. Kinematics of polygonal fault systems: observations from the northern North Sea. Frontiers in Earth Science, 5, 101.

www.mareano.no

www.npd.no, Norwegian Petroleum Directorate (NPD), Stavanger, Norway, 22.06.2021. Factpages of exploration wellbores, online. http://factpages.npd.no/factpages.

Figures and figure captions

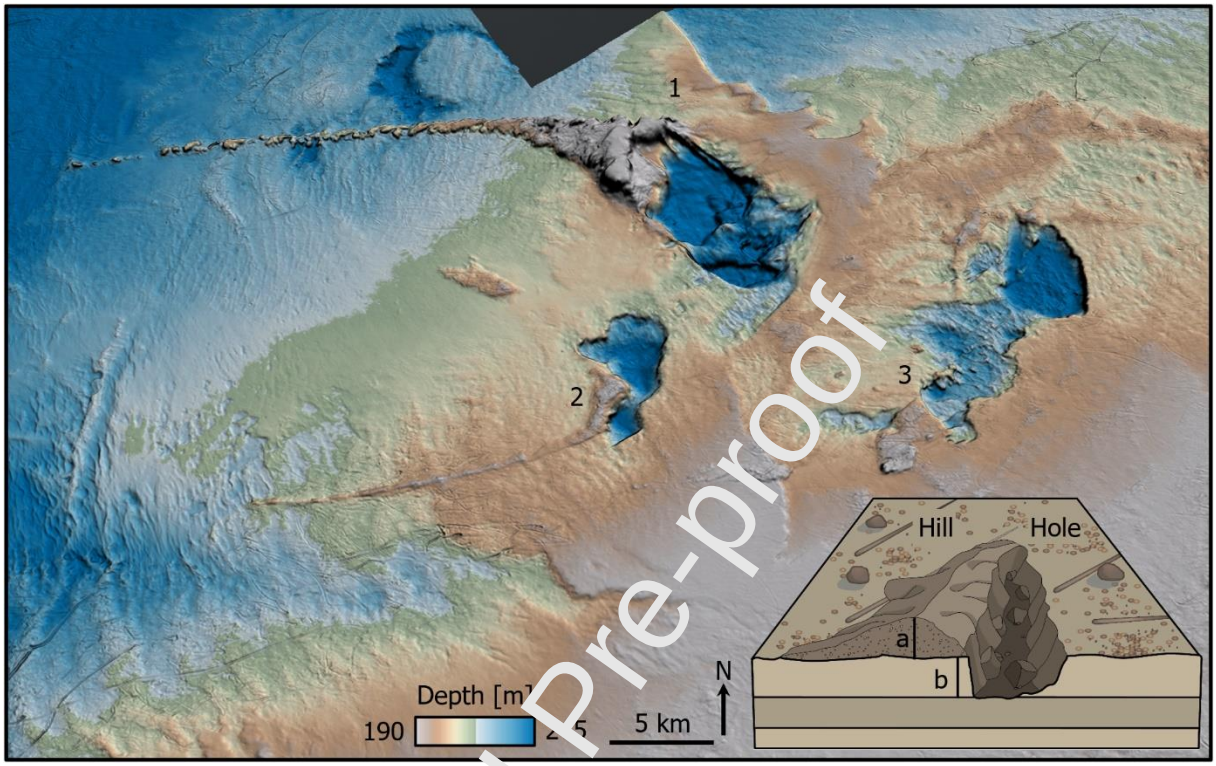

Fig. 1. Example of hill-hole pairs on modern seabed along a glaciated margin. Expression of the Steinbitryggen-Sopphola hill-hole pair at the modern seabed of the Tromsø Basin. The three hill-hole pairs in this area, indicated by numbers 1-3, are all characterized by a hill located to the west of the hole. Sketch in the lower-right corner shows how to characterize the dimensions of hill-hole pairs. Height of the hill (a) and depth of hole (b). Bathymetric data from mareano.no (cell size of 5x5 m). See Fig. 2 for location.

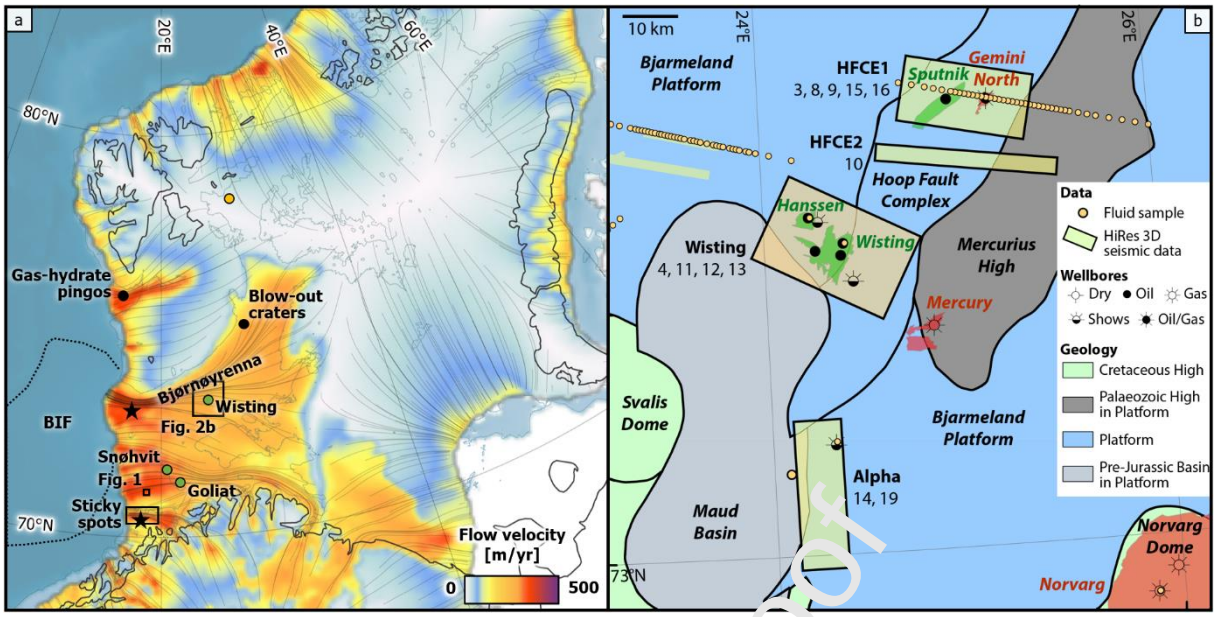

Fig. 2. Setting of the SW Barents Sea. **a)** Western Barents Sea Ice Sheet with modelled ice-flow velocities at Last Glacial Maximum (Patton et al., 2016), most prominent petroleum discoveries (green dots; www.npd.no), location of sticky spots (Winsborrow et al., 2016), blow-out craters (Andreassen et al., 2017), gas-hydrate pingos (Waage et al., 2019), cupola hills (black stars, Sættem, 1994), and hill-hole pairs of the central Barents Sea (yellow dot, Kurjanski et al., 2019). BIF: Bear Island Trough Mouth Fan. **b)** Datasets of the Greater Hoop area providing the basis of this study. Hydrocarbon discoveries (green: oil, red: gas) are shown. Numbers indicate figures generated from the seismic cubes. Rectangular shapes are HiRes 3D seismic datasets used in this study (names indicated as black text). Non-rectangular shapes are underlying geological units, with nomenclature indicated as black italic text. Geological information from npd.no.

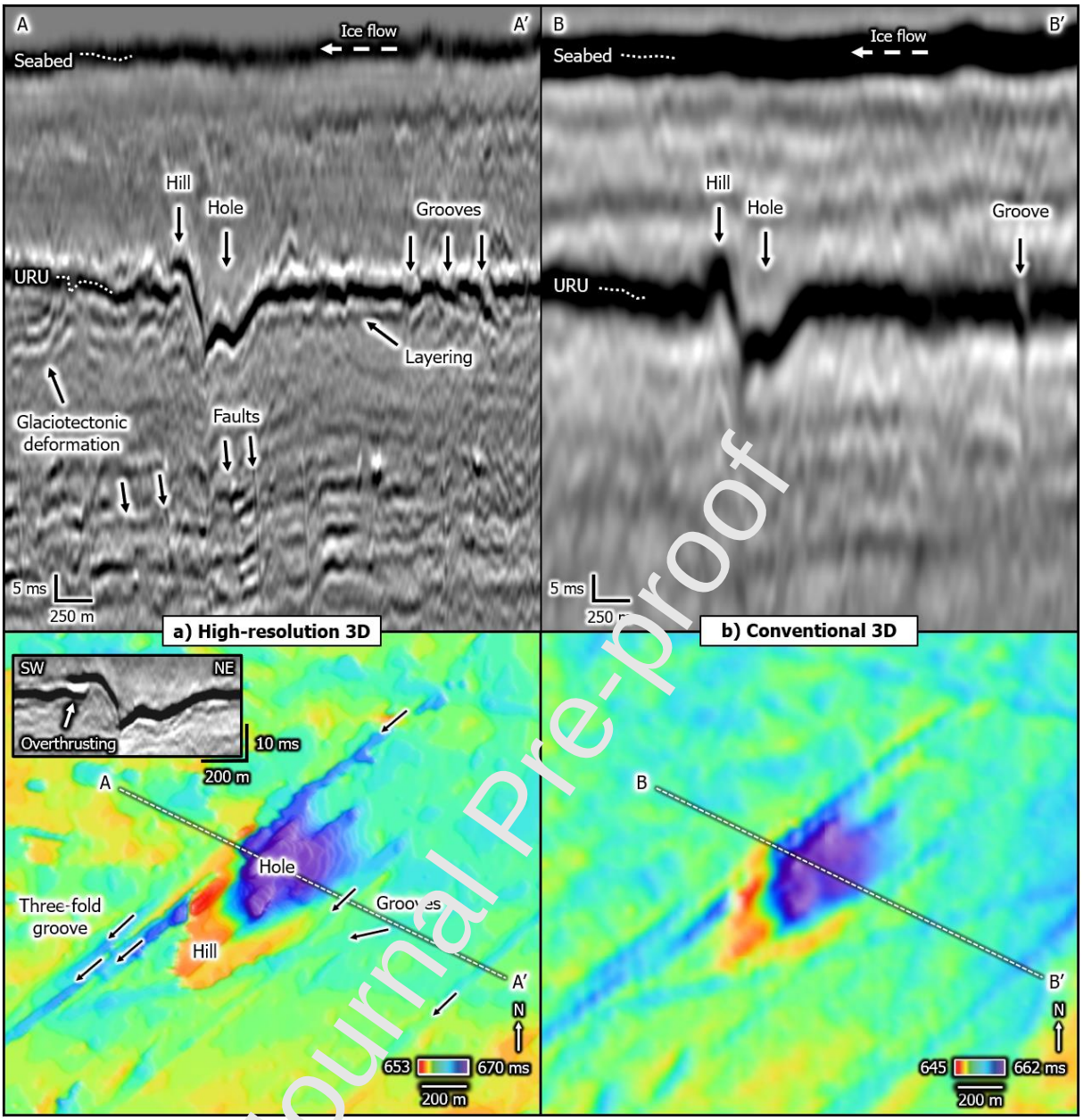

Fig. 3. Resolution improvements of high-resolution seismic data for hill-hole pair imaging along the URU surface and for underlying faults. **a)** Structure map of hill-hole pair using HiRes 3D seismic data (horizontal resolution of 6 m) and seismic profile across (vertical resolution of 3 m). **b)** Structure map of hill-hole pair using conventional seismic data (horizontal resolution of 12 m) and conventional 3D seismic profile across (vertical resolution of c. 12 m). URU is the prominent positive-amplitude reflection in the seismic profiles. Seismic inset shows overthrusting along the main axis of the hill-hole pair in high-resolution 3D seismic data. Seismic data courtesy of TGS and Fjorgyn.

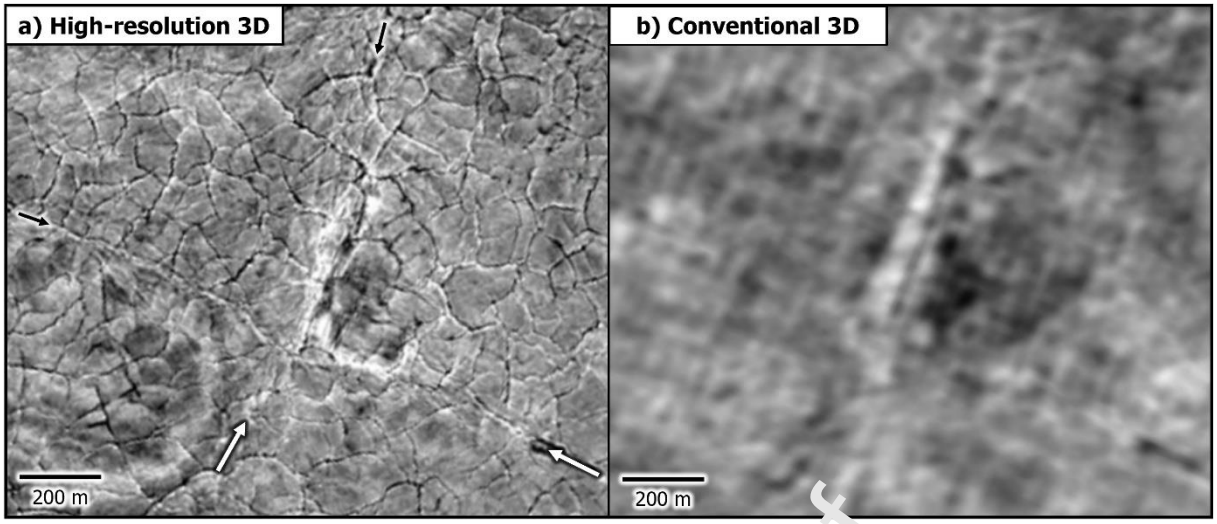

Fig. 4. Data comparison along time slice z = 496 m in the Wisting area. **a)** Deeper faults (arrows) and shallow faults (here polygonal) imaged by using high-resolution 3D seismic-amplitude data with a horizontal resolution of 3 m. **b)** Conventional 3D seismic amplitude data with a horizontal resolution of 12 m. The identification of the deeper faults is challenging, and the polygonal faults cannot be imaged. Seismic data courtesy of OMV and TGS.

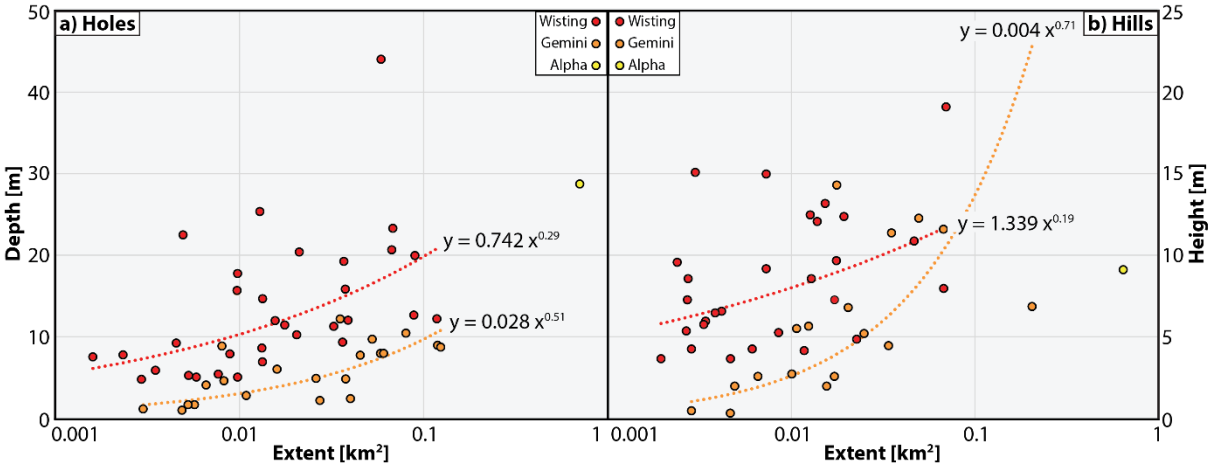

Fig. 5. Dimensions of hill-hole pairs identified in the high-resolution 3D seismic volumes from the Gemini North, Wisting and Alpha areas. Dataset shown in Supplementary Table 1.

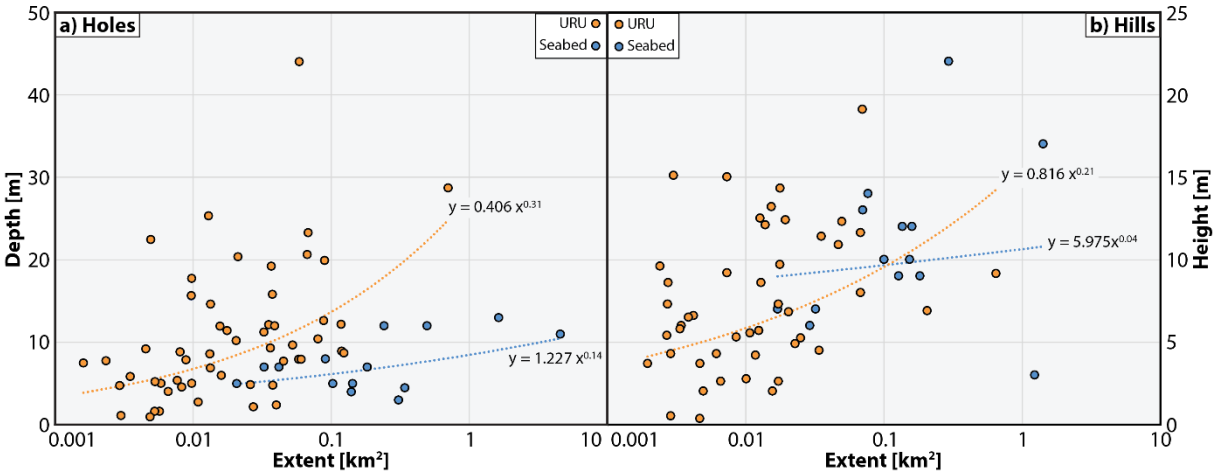

Fig. 6. Dimensions of hill-hole pairs identified at URU (this study, orange) compared to hill-hole pairs identified at the seabed of the central Barents Sea (Kurjanski et al. (2019), blue). Dataset shown in Supplementary Table 1.

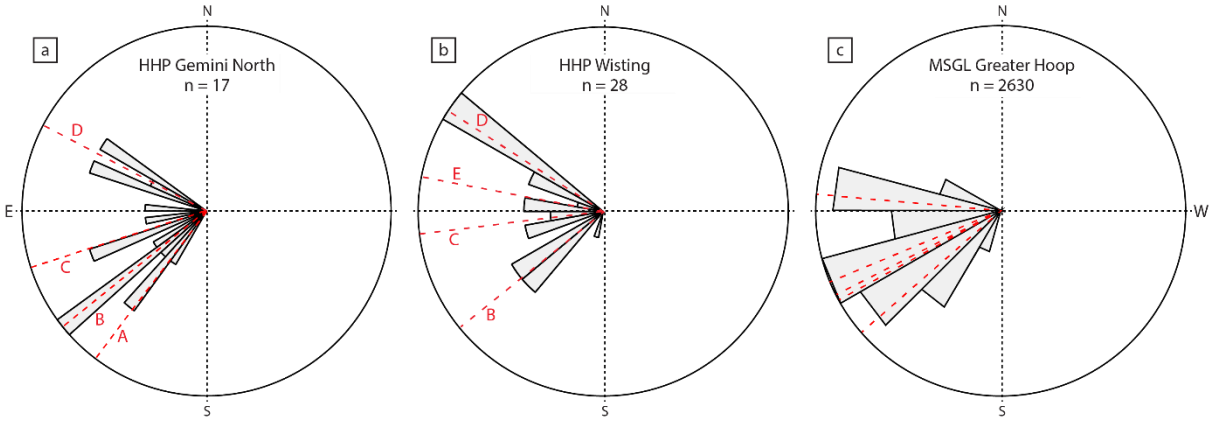

Fig. 7. Rose diagrams of hill-hole pairs (HHP) at URU. HHP identified in the high-resolution 3D seismic data of the Gemini North **(a)** and Wisting **(b)** areas. The red lines indicate average orientation, defining the clusters A, B, C, D and E. **(c)** Mega-scale glacial lineations (MSGL) at URU identified in conventional 3D seismic data of the Greater Hoop area, which includes the Gemini North area to the south. Data modified from Piasecka et al. (2016). Five ice-stream events are indicated by red stippled lines. Dataset shown in Supplementary Table 1.

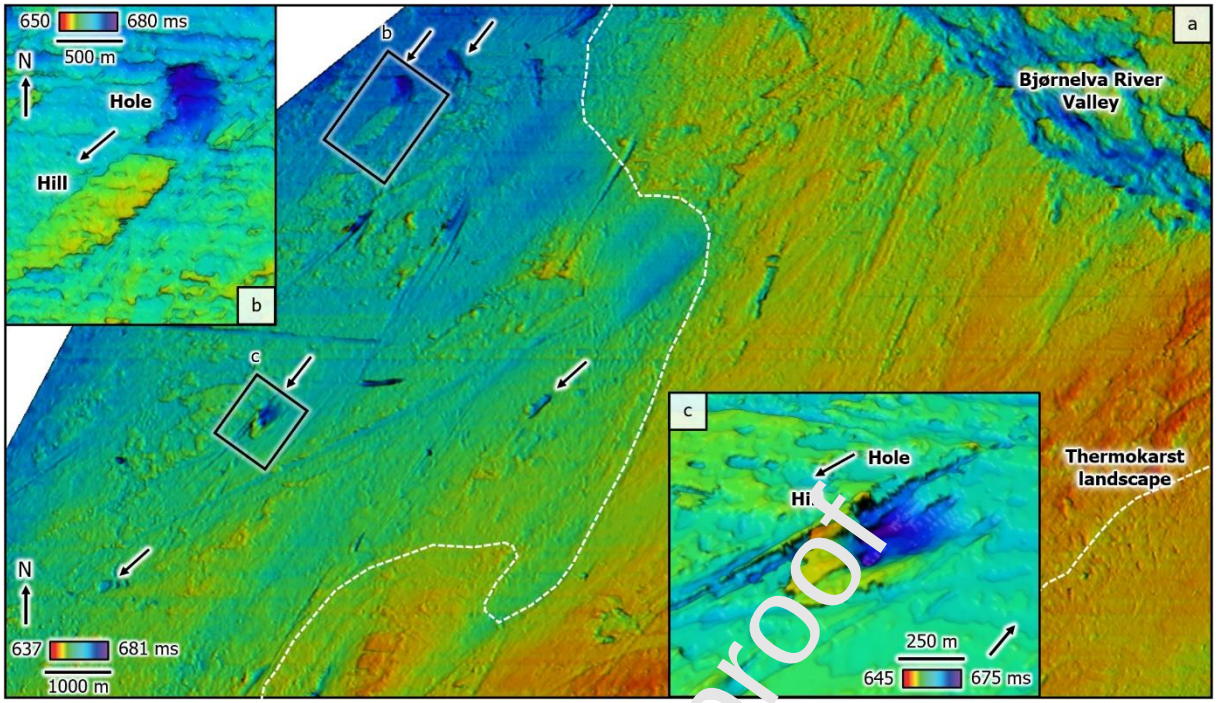

Fig. 8. Geomorphology of hill-hole pairs along buried surfaces. URU structure map of Gemini North area showing association between hill-hole pair orientation and ice streaming. **a)** URU structure map of the Gemini North area. Modified after Bellwald et al. (2019). Stippled line indicates extent of shear margin moraine (Bellwald and Planke,2019). Arrows show most prominent hill-hole pairs, which occur on the ice-streaming side of the shear zone. Hill-hole pair axis indicates dominant NE-SW ice streaming. **b)** Tabular hill-hole pair. **c)** Rimmed hill-hole pair. For seismic profile and planar view of this hill-hole pair, check Fig. 3a.

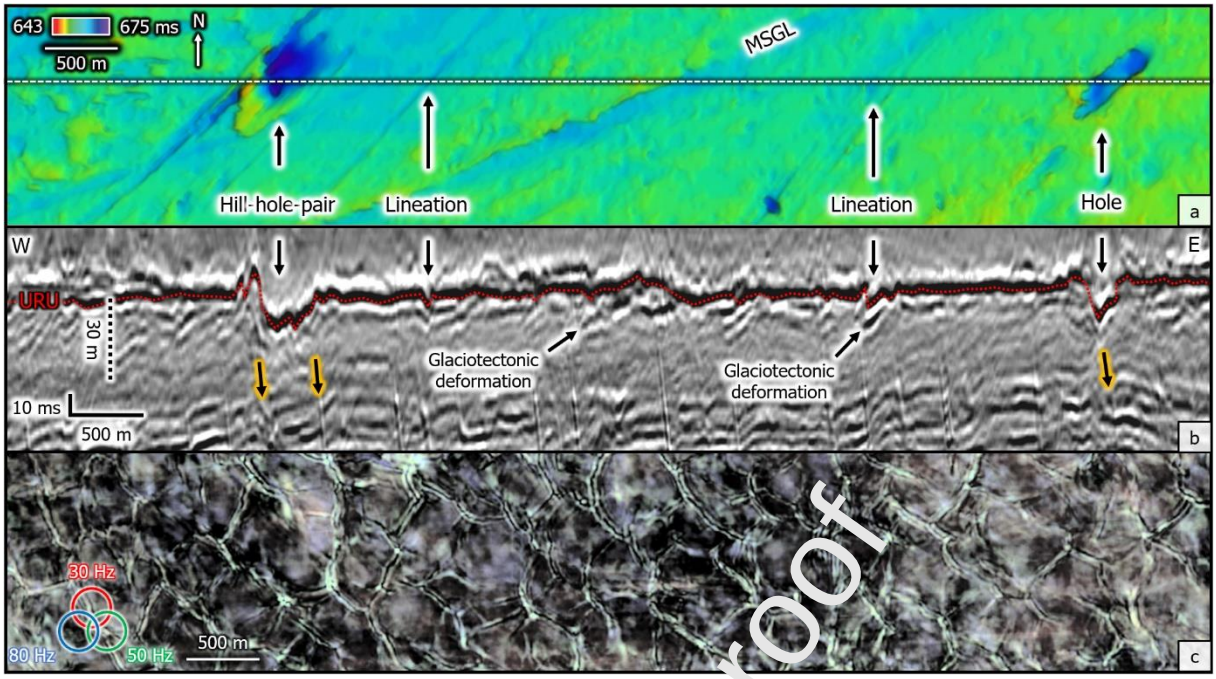

Fig. 9. Link between hill-hole pairs and faults in the shallow sub-surface of Gemini North area (HFCE1). **a)** URU structure map showing different glacial landforms. **b)** Seismic profile across glacial landforms. Yellow arrows indicate correlating polygonal faults. **c)** Frequency blending along time slice (t = 708 ms) to image polygonal faults. Black-colored areas indicate no frequency response. Seismic data courtesy of TGS and Fjorgyn.

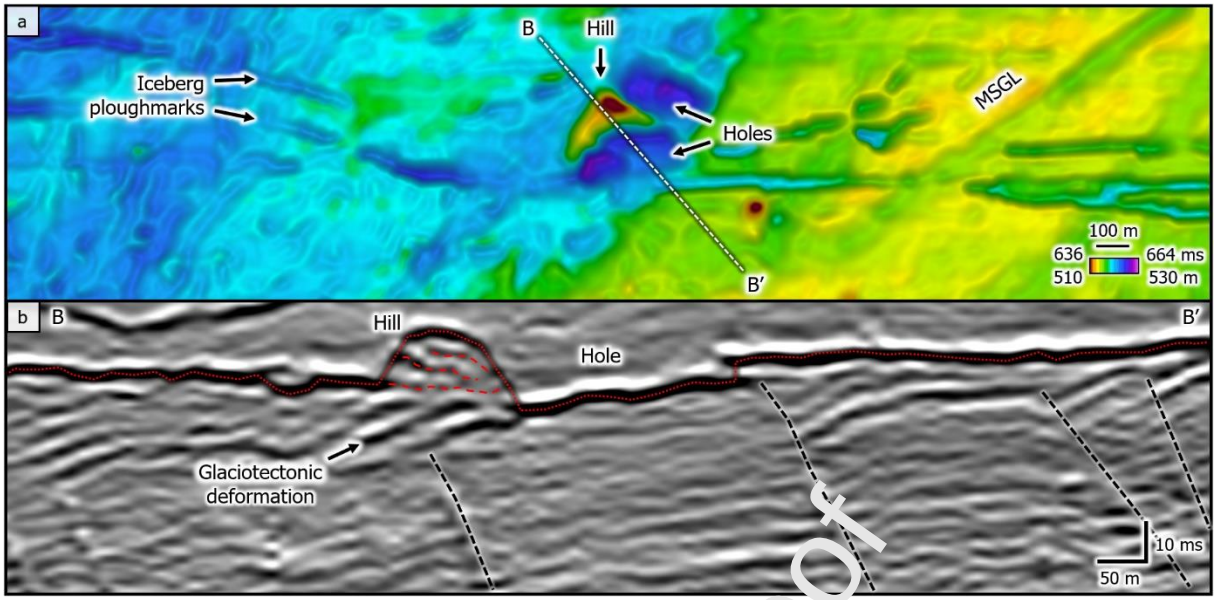

Fig. 10. Stratigraphy of hill-hole pairs. **a)** URU structure map of the Gemini North area (HFCE2). The hill-hole pair is characterized by two depressions separated by a 11 m high rim. Iceberg ploughmarks are predominantly east-westwards oriented. **b)** Internal layering of the hill and glaciotectonic deformation below URU. The location of the hole indicates a strong link with underlying faults. Seismic data courtesy of TGS and Fjorgyn.

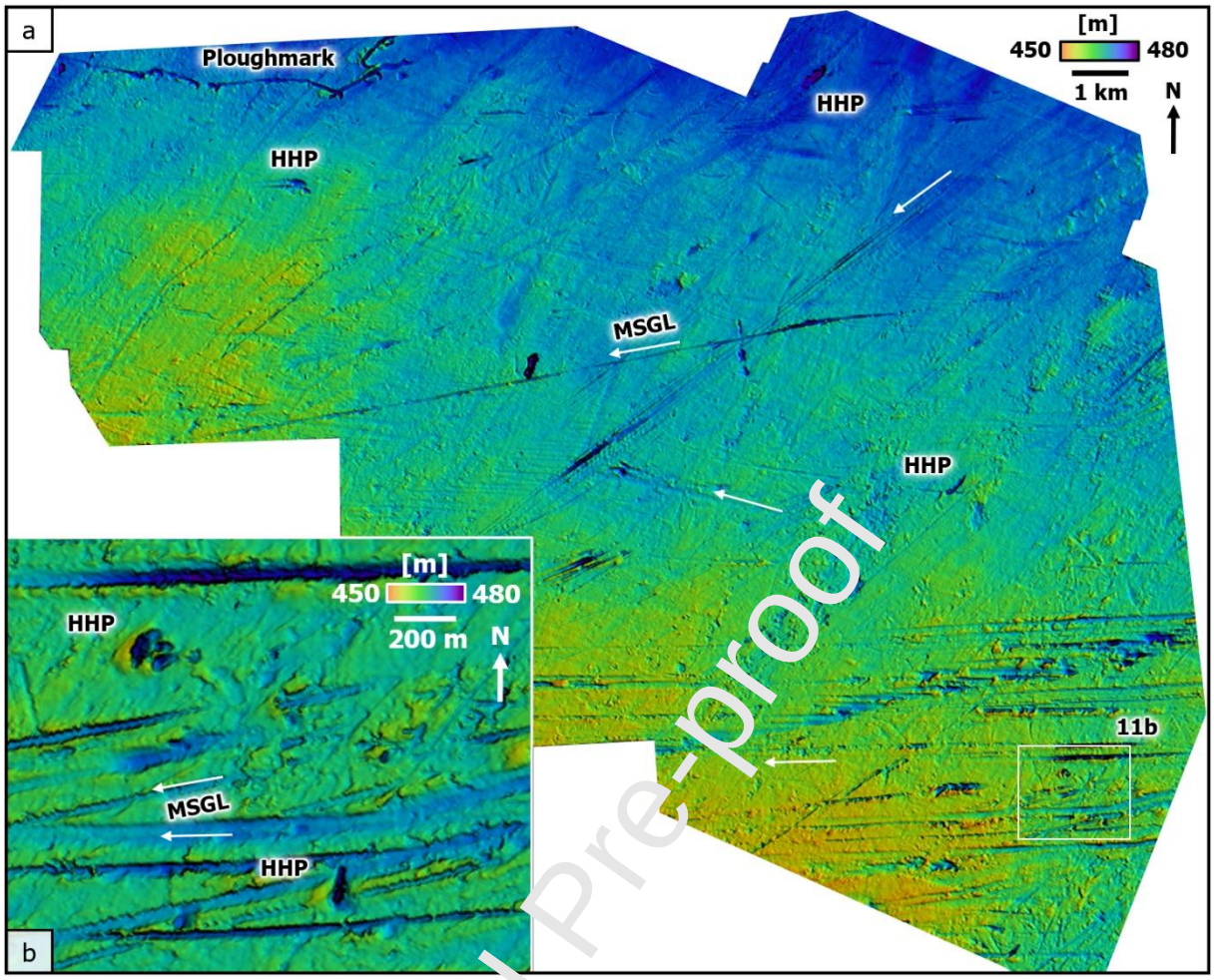

Fig. 11. Landform assemblages at UPU in the Wisting area. **a)** Structure map of the interpreted area. Four sets of mega-scale glacial lineations (MSGLs) are shown by white arrows. **b)** Zoomed image highlighting orientations of hill-hole pairs (HHPs) and mega-scale glacial lineations (MSGLs).

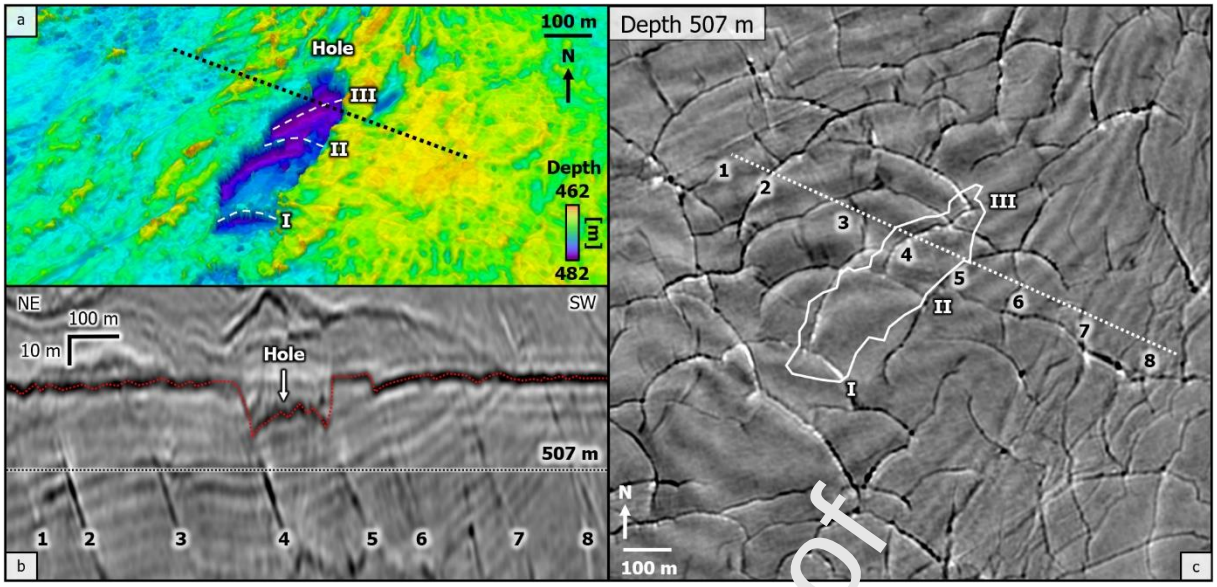

Fig. 12. Link between hill-hole pairs and underling polygonal faults. **a)** Structure map of a hill-hole pair at URU in the Wisting area. **b)** Seismic profile across the hill-hole pair. Polygonal faults are numbered. **c)** Time slice across polygonal faults at a depth of 507 m. I, II and III are polygonal fault segments. Seismic data access: DISKOS database, Norwegian Petroleum Directorate.

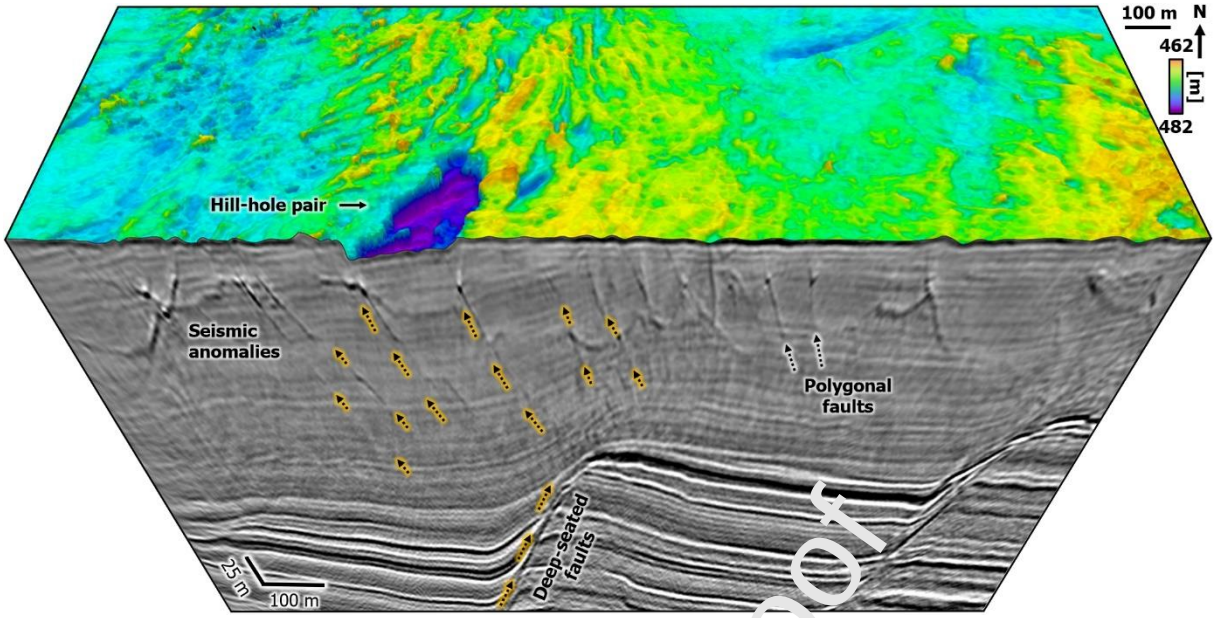

Fig. 13. Association between deeper faults, shallow faults and hill-hole pair in the Wisting area. Implied fluid migration along deep-seated and polygonal faults is shown by yellow arrows. Longer arrows along polygonal faults below hole indicate more focused fluid flow in this part, whereas fluids are also migrating along all other faults. Seismic data access: DISKOS database, Norwegian Petroleum Directorate.

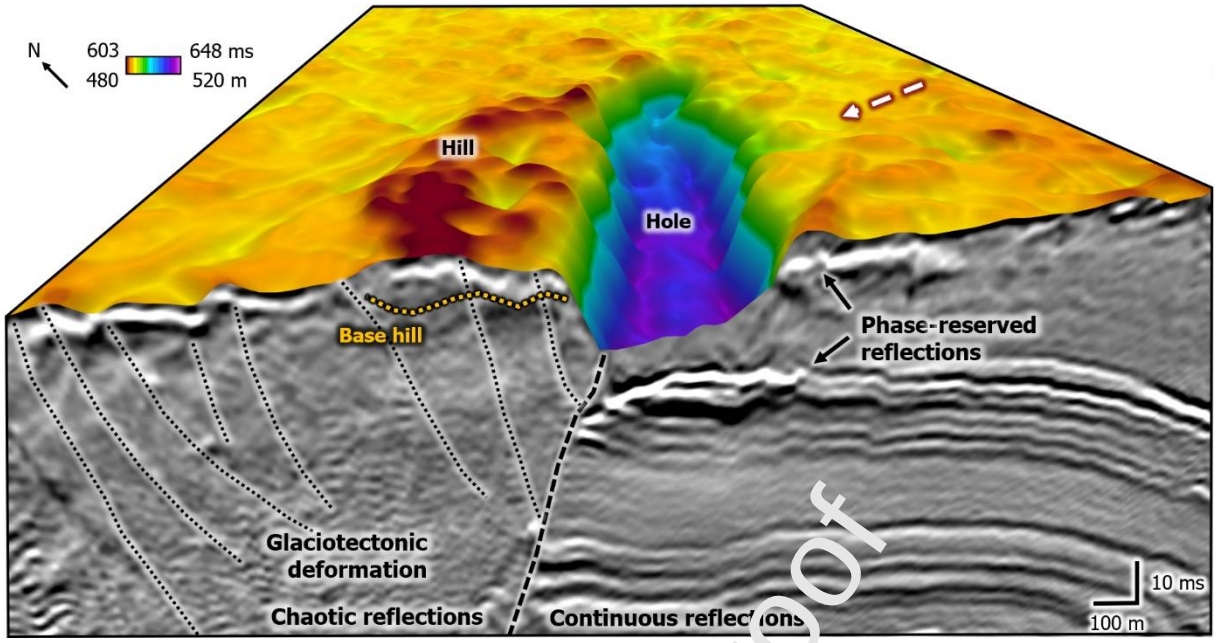

Fig. 14. Deeper faults and hill-hole pair in the Alpha area. Thick stippled line indicates deep Jurassic fault, whereas thin stippled lines show faults of likely glaciotectonic origin. Phase-reversed reflections below the hill-hole pair evidence the presence of shallow gas. White arrow indicates paleo-ice-streaming direction. Seismic data courtesy of TGS and Fjorgyn.

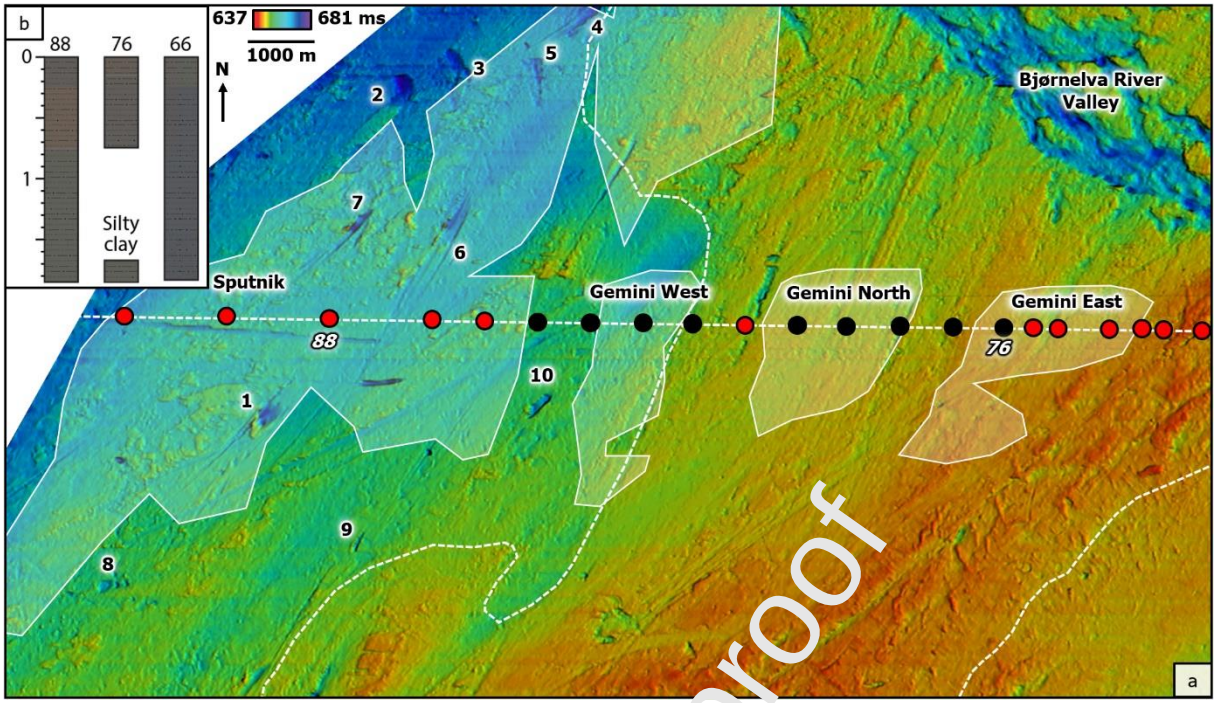

Fig. 15. Link between landforms at URU surface, seabed seep results, and Jurassic hydrocarbon reservoirs in the Gemini North area (HFCE1). **a)** Jurassic hydrocarbon reservoirs (white shaded areas), fluid seepage in seabed cores (red circles: anomalies, black circles: no anomalies), ten identified hill-hole pairs (numbers) and extent of shear margin moraine (white stippled line, modified after Bellwald and Planke, 2019) are indicated. **b)** Selected sediment cores for fluid seepage analyses. Numbers indicate core IDs. Sediment cores 88 and 76 are shown in Fig. 15a, whereas sediment core 66 is located 2.9 km to the east of the figure. Core data courtesy of TGS and VBER.

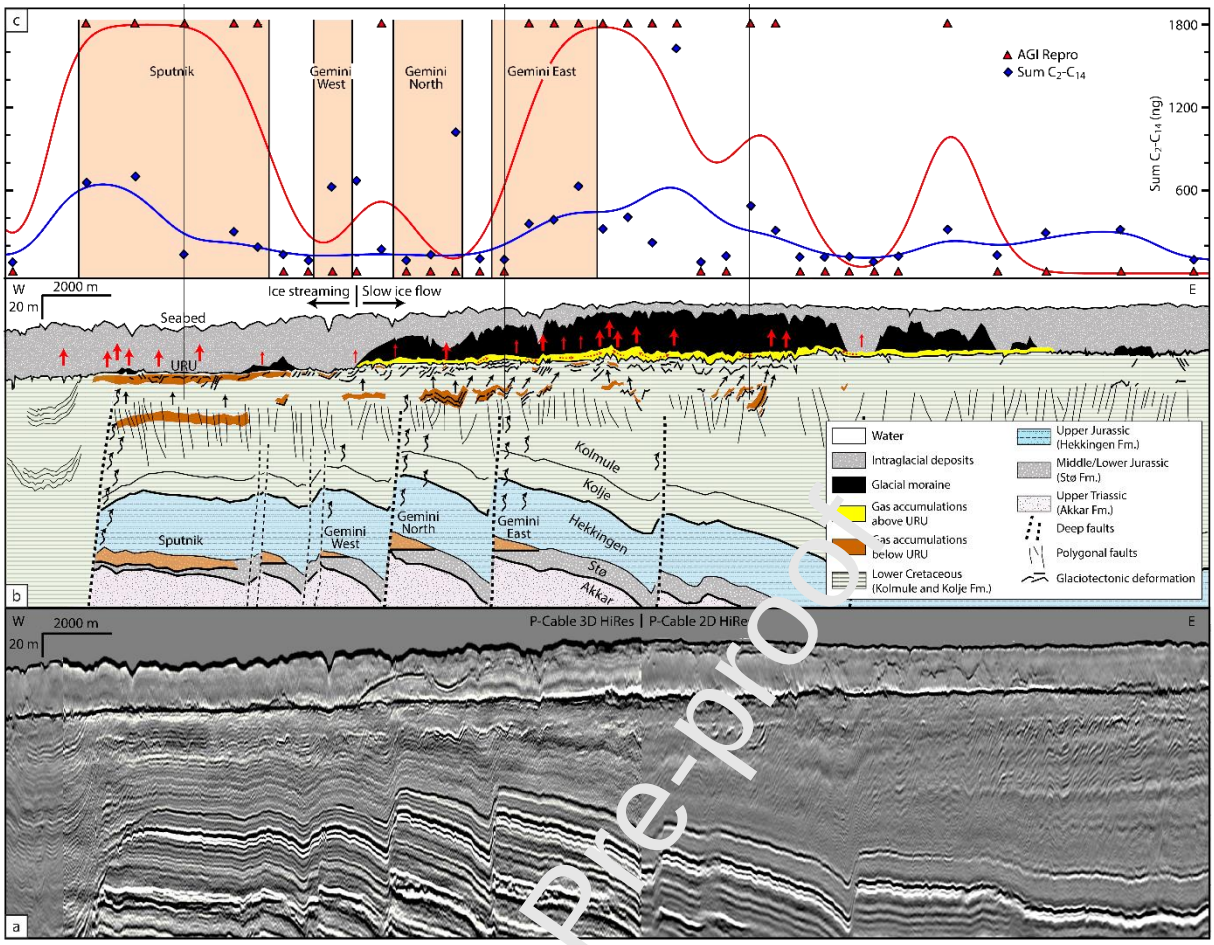

Fig. 16. Signature of fluid migration above different hydrocarbon fields. Hill-hole pairs only occur above the Sputnik field. **a)** P-Cable 3D high-res seismic profile across HFCE1 and P-Cable 2D high-res seismic profile outside of HFCE1. **b)** Interpreted seismic profile. Four hydrocarbon fields located within the Jurassic Stø Formation, of whom two have been drilled (Gemini North and Sputnik). Shallow gas is found at different stratigraphic levels above the reservoirs. Fluid migration within Mesozoic bedrock (black arrows) and Pleistocene glacial sediments (red arrows) is indicated. **c)** Results of fluid seepage from 37 sediment cores along the transect line. Red and blue lines show the seepage trends and are filtered within a window of 8 km. Seismic data courtesy of TGS and Fjorgyn; core data courtesy of TGS and VBER.

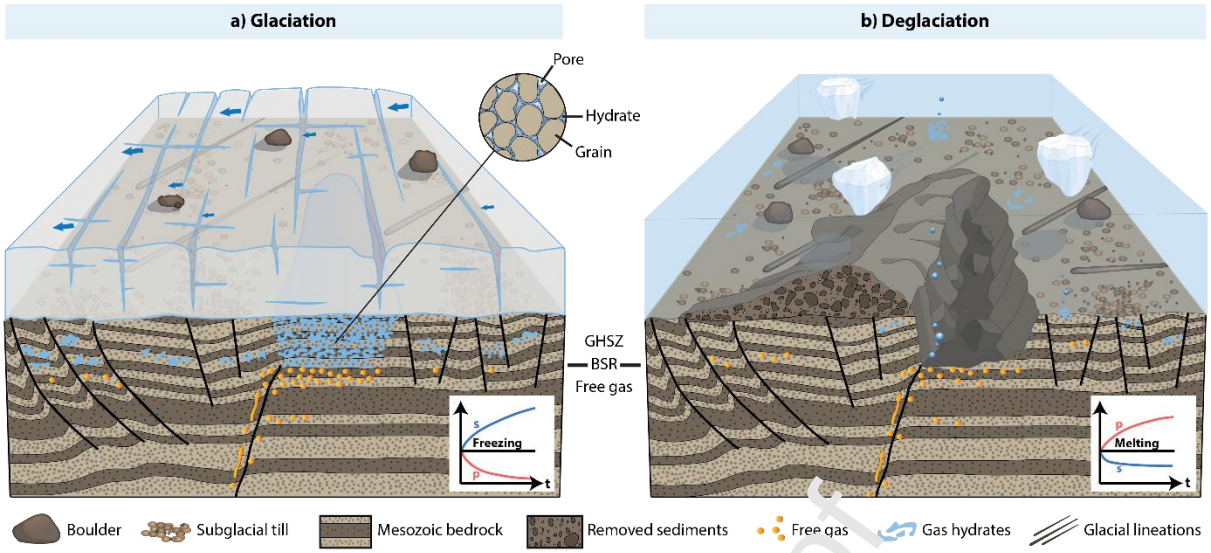

Fig. 17. Geological model for the formation of hill-hole pairs. **a)** Glaciated SW Barents Sea. Barents Sea Ice Sheet locally frozen to the underlying sedimentary bedrock, which is characterized by a deeper fault and polygonal faults with glaciotectonic deformation in the uppermost part. Gas hydrates are suggested to function as the glue for the freezing of the subsequently displaced bedrock, and faults to be locations of focused fluid migration. Fluids accumulate below the gas hydrate stability zone (GHSZ). Bjørnøyrenna Ice Stream flowing to the west transports underlying Mesozoic bedrock. Magnitude of ice streaming is indicated by blue arrows, with localized stagnation at the sticky spot. **b)** Hill formation: Ice flowing to the left released the Mesozoic bedrock evacuated from the hole (previous location of gas hydrates) and deposited it in the shape of a hill. Large quantities of gas hydrates dissociated, but gas accumulations may still be found close to the hole. Plots show time-dependent shear strength and shear stress (s, blue) and pore pressure (p, red) trends for freezing and melting stages. Plots are valid only for the glacier bed interface.

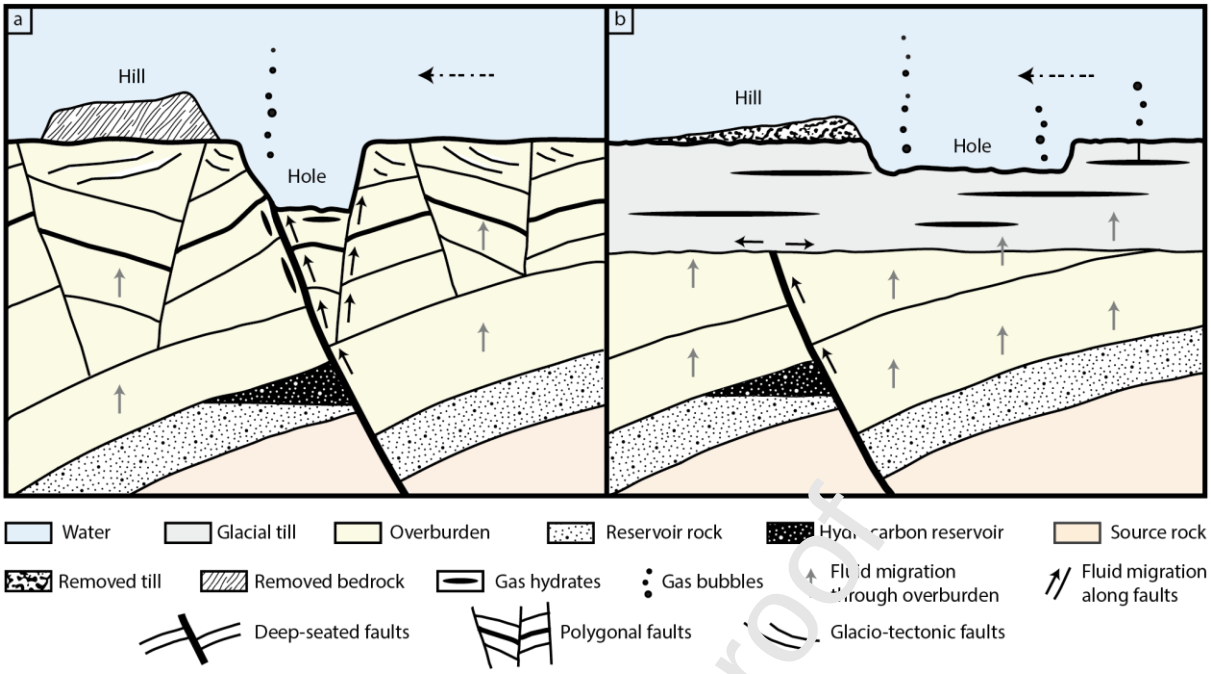

Fig. 18. Hill-hole pairs as hydrocarbon seep indicators. **a)** Hill-hole pair formed at an ice-bedrock interface (e.g., URU). Fluid migration from a hydrocarbon reservoir occurs along faults, which correlate with the holes. Glaciotectonic deformation may occur within the polygonal fault segments. **b)** Hill-hole pair formed at an ice-till interface (e.g., modern seabed). Fluid migration occurs both through overburden and along faults, and fluids can get laterally deviated at the till-bedrock interface.

Table 1. Relation between presence of hill-hole pairs at URU and fluid leakage from Jurassic hydrocarbon reservoirs. The information relates to the areas vertically above the reservoirs.

	Sputnik	**Gemini West**	**Gemini North**	**Gemini East**
Hill-hole pairs at URU	Yes	No	No	No
Negative anomalies below URU	High at multiple levels	Low	High	Moderate
Negative-amplitude anomalies above URU	Very low	Very low	High	Very high
Seepage to seabed	High	Low	Low	High
Ice configuration	Streaming	Streaming	Slow ice flow	Slow ice flow
Conclusion	Fluid leakage, formation of gas hydrates and hill-hole pairs at URU, fluid seepage to seabed ongoing	No fluid leakage, no gas accumulations	Fluid leakage, fluids accumulated below and above URU, lateral fluid migration at URU level	Fluid leakage, fluids accumulated below and above URU, fluid seepage to seabed ongoing

Graphical abstract

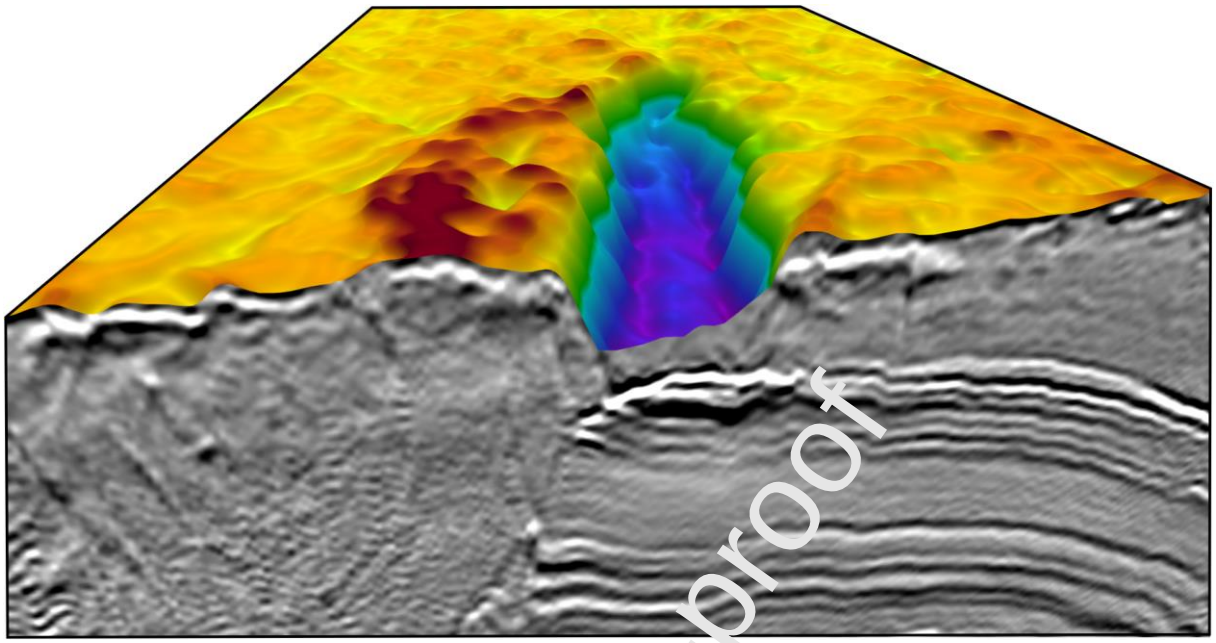

Highlights

- Hill-hole pairs have been studied along a glacial unconformity in the SW Barents Sea
- There is an association between buried hill-hole pairs thermogenic hydrocarbons
- Localized basal freezing of the Barents Sea Ice Sheet occurs near fault terminations
- Hill-hole pairs above bedrock indicate a link to faults and hydrocarbon reservoirs
- Hill-hole pairs can be used as hydrocarbon seep indicators in petroleum exploration